THE INVESTIGATION OF WARM LASER SHOCK PEENING AS A POST PROCESSING TECHNIQUE TO IMPROVE JOINT STRENGTH OF LASER WELDED MATERIALS

by

Gaurav Vilas Inamke

A Thesis

Submitted to the Faculty of Purdue University

In Partial Fulfillment of the Requirements for the degree of

Master of Science in Mechanical Engineering

School of Mechanical Engineering

West Lafayette, Indiana

May 2019

THE PURDUE UNIVERSITY GRADUATE SCHOOL
STATEMENT OF COMMITTEE APPROVAL

Dr. Yung C. Shin, Chair
School of Mechanical Engineering

Dr. Benxin Wu
School of Mechanical Engineering

Dr. Gary J. Cheng
School of Industrial Engineering

Approved by:

Dr. Jay P. Gore
Head of the Graduate Program

Dedicated to my family

ACKNOWLEDGMENTS

I would like to express my sincere gratitude to my academic advisor Dr. Yung C. Shin for being a great source of inspiration, perseverance and determination in ensuring my success throughout my course of study at Purdue. His motivation, diligent guidance and mentoring has empowered me to expand my horizons and learn holistically during my Master's program. I am grateful to him for introducing me to the amazing field of lasers and for expanding my skill set with state of the art equipment and facilities.

I sincerely thank Dr. Yung C. Shin, Dr. Benxin Wu and Dr. Gary J. Cheng for serving on my advisory committee and for sparing their invaluable time reviewing my thesis.

I thank my lab mates, colleagues and friends at Purdue who made my stay here memorable. A special thanks to Ms. Jennifer Hall at the Brian Lamb School of Communication who provided me with the opportunity to work as a Graduate Teaching Assistant.

I want to deeply thank my father Vilas, my mother Anita and my sister Namrata for their unshakable faith in my abilities, their constant support and encouragement through tough times. You have made immeasurable sacrifices in ensuring that I succeed and for that, I am forever grateful.

Finally, I want to deeply thank my wife Girija for her determination, understanding and for being a calming presence whenever I was in turmoil. Your belief in my abilities allowed me to forge ahead.

TABLE OF CONTENTS

LIST OF TABLES

LIST OF FIGURES

ABSTRACT

Author: Inamke, Gaurav, V. MS
Institution: Purdue University
Degree Received: May 2019
Title: The Investigation of Warm Laser Shock Peening as a Post Processing Technique to Improve Joint Strength of Laser Welded Materials
Major Professor: Yung C. Shin

This study is concerned with investigating the effects of warm laser shock peening (*w*LSP) on the enhancement of mechanical performance of laser welded joints. A 3-D finite element model is presented which predicts the surface indentation geometry and in-depth compressive residual stresses generated by *w*LSP. To define the LSP pressure on the surface of the material, a 1-D confined plasma model is implemented to predict plasma pressure generated by laser-coating interaction in an oil confinement regime. Residual stresses predicted by the finite element model for *w*LSP reveal higher magnitude and depth of compressive residual stresses than room temperature laser shock peening. A novel dual laser *w*LSP experimental setup is developed for simultaneous heating of the sample, to a prescribed temperature, and to perform *w*LSP. The heating laser power is tuned to achieve a predefined temperature in the material through predictive analysis with a 3-D transient laser heating model.

Laser welded joints of AA6061-T6 and TZM alloy in bead-on-plate (BOP) and overlap configurations, created by laser welding with a high power fiber laser, were post processed with *w*LSP. To evaluate the strength of the welded joints pre- and post-processing, tensile testing and tensile-shear testing were carried out. To understand the failure modes in tensile-shear testing of the samples, a 3-D finite element model of the welded joint was developed with weld regions' material strength properties defined through microhardness testing. The stress concentration regions predicted by the finite element model clearly explain the failure regions in the experimental

tensile testing analysis. The tensile tests and tensile-shear tests carried out on *w*LSP processed AA6061-T6 samples demonstrate an enhancement in the joint strength by about 20% and ductility improvement of about 33% over as-welded samples. The BOP welds of TZM alloy processed with *w*LSP demonstrated an enhancement in strength by about 30% and lap welds demonstrated an increase in joint strength by 22%.

1. INTRODUCTION

1.1 Rationale

The mechanical performance of laser welded materials has been an area of concern in the industry. Difficult-to-weld materials such as Aluminum alloys and Molybdenum alloys have a considerable drop in strength when welded using fiber lasers. Porosity is one of the primary reasons for reduction in joint strength. For tough materials like Ti-Zr-Mo alloys, in addition to porosity, welded joints are marred by low joint strength due to a loss of plasticity and brittle failure under mechanical loading. For the restoration of the weld strength, post weld treatments such as post weld ageing treatment, stress relief annealing heat treatment, cold rolling and shot peening have been implemented in the past with some success. However, these methods have inherent limitations such as high processing times, high surface roughness, low depth of compressive residual stresses as well as inaccessibility to areas in a part with complex geometry.

Laser Shock Peening is a surface modification technique that has been perfected over a time period of two decades by the scientific community. Laser Shock Peening (LSP) is a very effective surface processing technique that is used to treat metals for enhanced fatigue life, better surface strength, along with improved wear and corrosion resistance. The advantages of LSP over other conventional fatigue life enhancement processes viz. shot peening, ultrasonic impact peening, etc. include: (1) higher magnitude and depth of compressive residual stresses, (2) the ability of processing complex surface geometries on components, and (3) the ability to control the depth and magnitude of the compressive residual stresses imparted in the material by virtue of highly accurate finite element analysis. Laser Shock Peening (LSP) processed materials benefit from higher fatigue life, higher stress corrosion resistance along with a better surface finish [1].

While LSP has many advantages, it also faces a few major challenges. Under mechanical loading or thermal heating, the compressive residual stresses induced by LSP are prone to relaxation. As these compressive residual stresses are the primary mechanism of fatigue life enhancement, the relaxation of these residual stresses is an undesirable characteristic. The primary mechanisms responsible for this residual stress relaxation are: (1) compressive or tensile over loading, (2) cyclic loading in the vicinity and above the endurance limit, and (3) exposure to thermal cycling. These practical limitations can be alleviated by a process known as warm laser shock peening (*w*LSP). The novel process of *w*LSP was first developed by Ye et al. [2] in 2010. *w*LSP involves heating up the target material to a certain processing temperature and subsequently processed with LSP. *w*LSP is a thermo-mechanical surface processing method, which combines the advantages of LSP, dynamic strain aging (DSA) and dynamic precipitation (DP) to create highly stable microstructures. With the combined effect of DSA and DP, the dense dislocations are generated along with highly dense nano precipitates. Under thermal or mechanical loading, the precipitates and diffused solute atoms resist movement of nearby dislocations, creating a dislocation pinning effect. This effect improves the stability of the residual stresses generated and enhances the mechanical performance of the processed materials.

Therefore, laser welded joints are of interest for the application of LSP and *w*LSP as a post processing technique to enhance mechanical properties.

One of the common and yet time consuming method of restoring weld strength is post weld ageing. Malarvizhi and Balasubramanian [10] reported 11% improvement in tensile strength for FSW AA2219 aluminum alloy joints processed with post weld ageing at 175°C. The increase in joint strength was found to be due to the existence of dense precipitates, by virtue of ageing, that

hamper movement of dislocations (dislocation pinning). However, the duration of this ageing process was 12 hours and hence in industrial applications, post weld ageing is not a practical solution for joint strength enhancement. Dynamic ageing or dynamic precipitation is a high-speed precipitation process that generates precipitates in materials in a much shorter time frame. *w*LSP is a process that induces DSA and DP in materials and is therefore an attractive alternative to increase the joint strength of laser welded joints. Su et al. [11] processed TIG welded AA6061-T6 with LSP in the DSA temperature regime and reported a 40% increase in fatigue life. The practical limitation of WLSP reported in literature is the use of a heating pad to heat the material. For laser welded joints with complex geometry, the use of a heating pad is impractical. It is therefore necessary to develop an industrially viable solution for processing laser welded joints with *w*LSP to enhance its mechanical performance.

This study is concerned with the *w*LSP processing of laser welded joints using a novel dual laser arrangement. The primary aim of this study is to evaluate the improvement in mechanical performance for laser welded lap joints and bead on plate joints using a very fast *w*LSP process.

1.2 Literature Review

1.2.1 Laser Shock Peening

Laser Shock Peening (LSP) is a surface modification process that imparts beneficial compressive residual stresses into the target material to assist in improving its fatigue life. In LSP, the target material is coated with an opaque ‘sacrificial’ coating layer, which serves to protect the target material from any thermal damage caused by laser irradiation. A transparent ‘confinement’ overlay viz. water, glass, oil is then placed over the surface of the material and a high energy laser pulse is irradiated on the target surface through the transparent overlay. This irradiation results in the ablation of the sacrificial coating layer and the generation of high pressure plasma in the

confinement region. This plasma also causes a high pressure shockwave to propagate into the target material, which imparts compressive residual stresses into the material, predominantly in the surface region [12]. A schematic of the Laser Shock Peening process is shown in Figure 1.1. The physics of the confinement effects of the plasma generated has been studied extensively in literature. Fabbro et al. [13] proposed a 1-D analytical model considering the plasma pressure generated by a glass transparent overlay. Zhang et al. [14] improved upon this model later. However, the major shortcomings of this model were that it had multiple free variables that had to come from experimental measurements. Wu and Shin [15]developed a self-closed thermal model that predicted plasma pressure under water confinement. The standout advantage of this model is that it has no free variables and has included the most important physical phenomena including the water evaporation, ablation of the sacrificial layer, plasma ionization and expansion, laser-plasma interaction, etc.

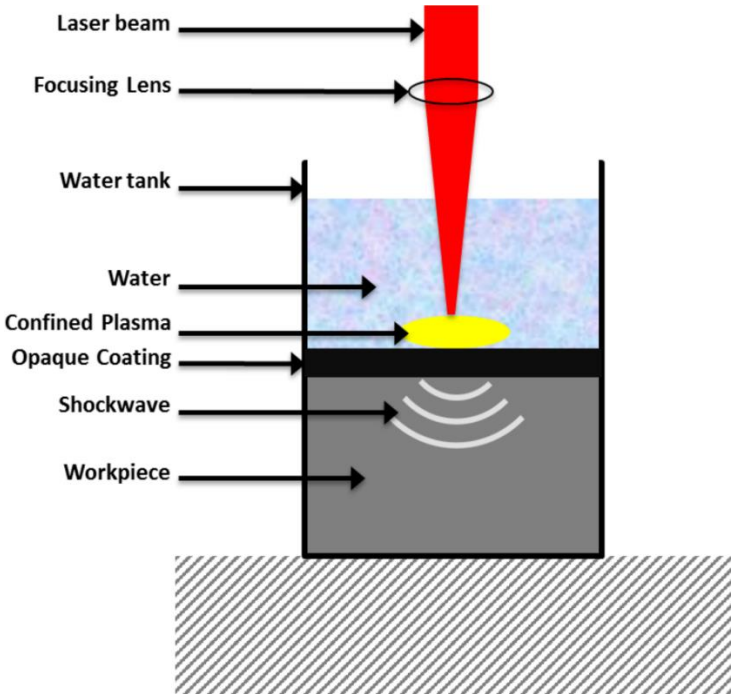

Figure 1.1. Schematic representing Laser Shock Peening

The finite element modeling of laser shock peening has been reported in literature extensively [12, 16, 17]. In these studies, the modeling approach involves combining ABAQUS/Dynamic and ABAQUS/Static to simulate the high speed short duration shock wave propagation through the material and the resulting residual stresses imparted in the material. However, most previous studies used the 1-D analytical model proposed by Fabbro et al. [13] which relies on two free variables that are obtained from experimental measurements. Cao and Shin [18] carried out finite element modeling of LSP using the confined plasma model developed by Wu and Shin [19] as the input for calculating plasma pressure generated during LSP in a water confinement regime. The authors developed a 3D finite element model for predicting the residual stresses in LSP processed materials and reported high prediction accuracy when validated with experimental data for a range of materials and processing parameters.

The primary objective of LSP is to impart beneficial residual stresses which enhance the fatigue life of the processed material. The high strain rate deformations caused by the shockwave propagating into the material causes the generation of dense dislocations in the surface region of the material. During mechanical loading, these dense dislocations cause dislocation tangles, which result in strengthening of the material. However, under excess cyclic loading at or near the endurance limit, there is a residual stress relaxation in the subsurface of the LSP processed materials which is detrimental to its fatigue life. Also, due to the work hardening induced by LSP, there is a loss of ductility in the material.

1.2.2 Warm Laser Shock Peening

The wLSP processing technique involves elevating target material temperature to the dynamic precipitation regime and subsequently processing the material surface with LSP. Compared to room temperature LSP (rtLSP), *w*LSP induces highly stable, deeper residual

compressive stresses in the processed material, which cause material strengthening without loss of ductility. *w*LSP has been researched for a range of materials such as aluminum alloys, steels and titanium alloys. Ye et al. [2] carried out *w*LSP of AA6061-T6 and reported improved fatigue life in the high cycle region of *w*LSP samples with better stability of residual stresses as shown in Figure 1.2. The AA6061-T6 *w*LSP processed specimen also contained ultrafine dense nanoprecipitates and dense dislocations that contribute towards the improved mechanical performance. In another investigation, Ye et al. [21] processed AA7075 with *w*LSP and reported a 32.3% improvement in material strength than rtLSP with no additional loss of ductility. For *w*LSP processing of AISI 4140, Ye et al. [22] reported the presence of ultrafine carbide precipitates in the processed samples. Thermal stability of the residual stresses generated due to *w*LSP also improved high temperature fatigue performance of the processed AISI4140. Zhou et al. [23] processed Ti6Al4V with *w*LSP and reported a greater depth of compressive residual stresses than rtLSP samples.

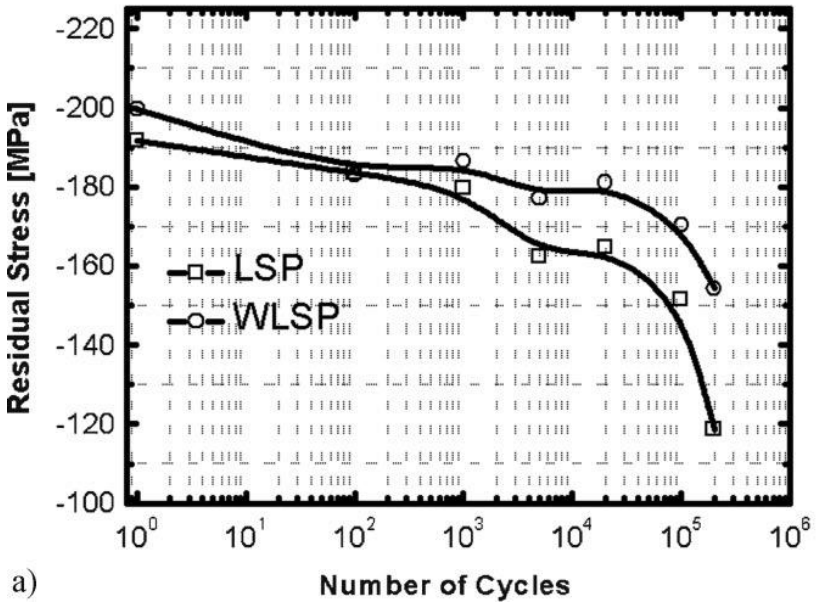

Figure 1.2. Improved cyclic stability of compressive residual stresses generated by wLSP in AA6061-T6, adopted with permission from [2]

Liao et al. [24] investigated the fundamental mechanism of material strengthening in *w*LSP and reported that due to the DSA effect more tangled dislocations with a uniform distribution are generated, since dislocation multiplication is promoted. The combined thermal and mechanical energy during *w*LSP promotes diffusion of carbon atoms, which leads to the formation of a high concentration of carbon atoms near dislocation cores. These dislocation cores provide nucleation sites for the generation of nanoprecipitates. The DA effect thereafter results in the generation of high density globular nanoprecipitates with a size of around 3-10nm in these nucleation sites. Under mechanical loading of *w*LSP processed materials, the dislocation – precipitate interaction and the Orowan effect [25]of strengthening are the primary mechanisms of material strengthening. The dislocation pinning effect, which is caused due to the resistance to dislocation movement caused by precipitates, results in higher stability of the dislocations generated. These highly stable dislocations contribute towards higher stability of the compressive residual stresses, thereby increasing the fatigue life of the material.

Owing to the improved material strength, no reduction in ductility and significantly higher fatigue life due to stable residual stresses, *w*LSP is a very promising post-processing technique.

1.2.3 Weld Strength of Laser Welded Joints for AA6061-T6 and TZM alloy

Material joining techniques such as fusion welding and solid-state welding are widely used for producing products in industry. The various methods of joining metals together include but are not limited to resistance welding, tungsten inert gas welding, metal inert gas welding, electron beam welding, friction stir welding and laser welding. While these processes have been in use for a very long time, with highly sophisticated equipment and advanced techniques, there still remains a great difficulty in predicting and achieving the desired quality of welds. Welding is a complex process in which a weld joint undergoes thermal, mechanical, metallurgical and microstructural

changes. Evaporation of alloying elements, changes in chemical composition and microstructure of alloys, porosity and resultant residual stresses after welding significantly affect the quality of the welded joint. Compared to conventional welding methods such as tungsten inert gas (TIG) welding, metal inert gas (MIG) welding and friction stir welding, laser welding offers advantages such as high weld speed, narrow heat affected zones, better weld quality and mechanical properties of weld joints [26]. Despite these advantages, laser welding of difficult to weld materials such as aluminum alloys and molybdenum alloys is still problematic and there is a pressing need to improve the joint strength of laser welded joints.

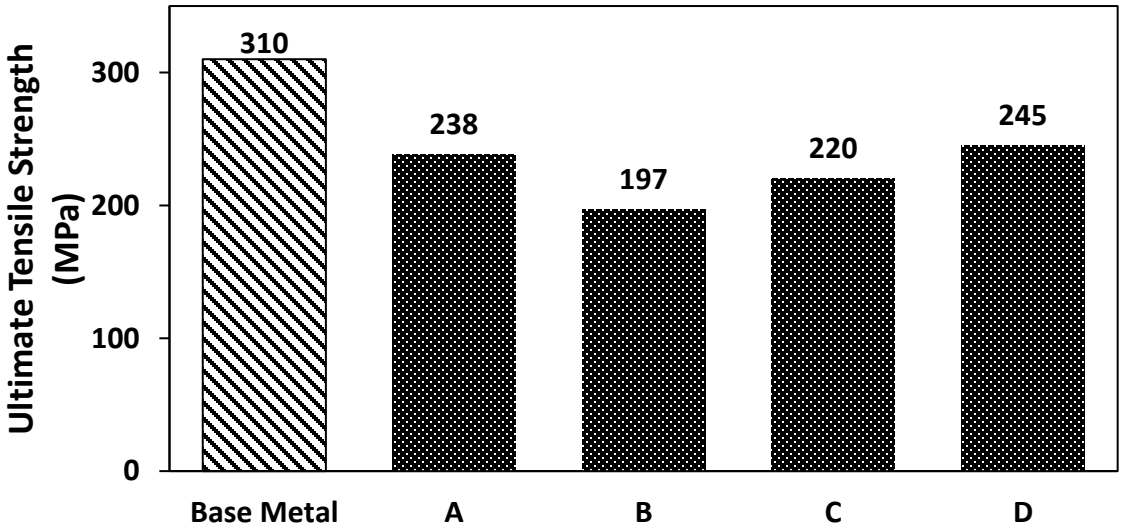

Sr. No.	Material Thickness	Filler Material	Source
A	2 mm	-	Padmanabham and Shanmugrajan [27]
B	2 mm	-	Narsimhachary et al. [28]
C	1 mm	AA4043	El-Batahgy and Kutsuna [29]
D	2 mm	-	Hirose, Todaka and Kobayashi [30]

Figure 1.3. Ultimate Tensile strength of laser welded AA6061-T6 joints

For laser welded AA6061-T6 alloy, weld strength is a critical concern since there is a considerable drop in the material strength at the joint [31, 32] as shown in Figure 1.3. Porosity is

one of the primary reasons for the reduced mechanical strength of the welds [31, 32]. Padmanabham et al. [27] reported a joint strength of ~65% compared to that of the base metal for laser welded bead-on-plate welds of AA6061-T6. Narsimhachary et al. [28] reported low hardness in the fusion zone of the Al 6061-T6 weld specimens and a tensile strength of 197±20 MPa for bead-on-plate laser welded joints compared to the tensile strength of 300MPa for the base metal. Chu et al. [33] investigated weld strength of laser welded AA6061-T6 with filler material and reported joint strengths in the range of 94-107 MPa. El-Batahgy and Kutsuna [29] reported presence of porosity and solidification cracking in welded specimens of AA6061-T6. Hirose et al. [30] investigated the joint strength of laser welded AA6061-T6 bead-on-plate welds and reported about 70% weld strength to that of the base metal. The authors also processed the welds with post weld ageing and reported about 15% improvement in weld strength. Earlier studies however mainly focused on bead-on-plate and butt weld configurations. There has been less focus on the joint strength of laser welded lap joints. Kim et al. [34] reported that partial penetration of weld pool in lap welded Al 5052 resulted in greater porosity. However the strength of the welded joints was not reported. A recent study by Pellone et al. [35] reported that for laser welded AA6061-T6 lap joints, the addition of an interface gap resulted in low porosity, good appearance and strong lap welds.

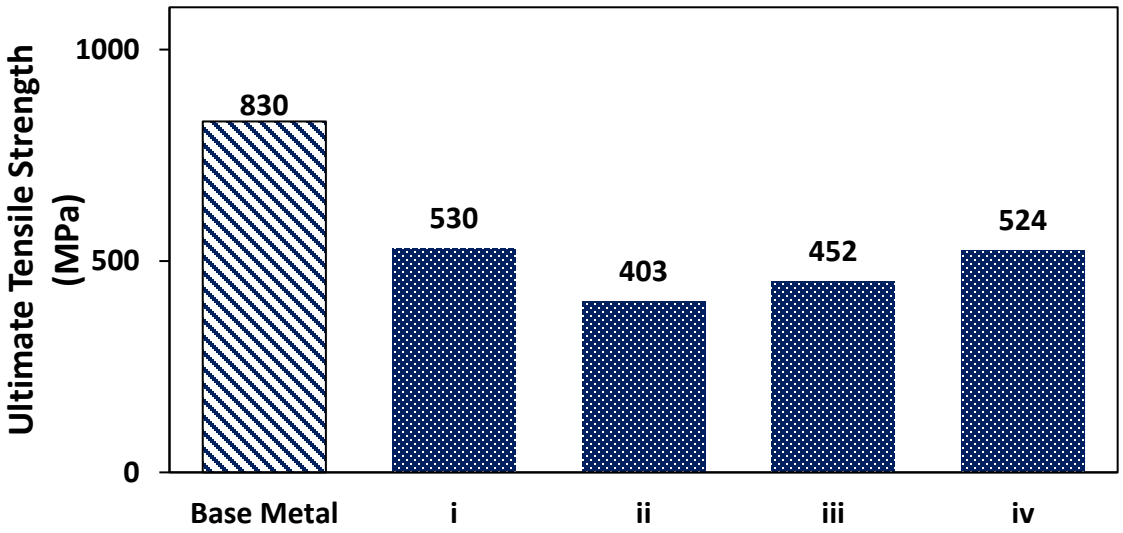

Sr. No.	Material Thickness	Welding Process	Source
i	2 mm	EBW	Stütz et al. [36]
ii	3 mm	EBW	Wang et al. [37]
iii	3 mm	EBW	Wang et al. [38]
Iv	3 mm	EBW	Zhang et al. [30]

Figure 1.4. Ultimate tensile strength of welded TZM alloy joints

TZM is a molybdenum based alloy that has high strength at high temperatures, high thermal conductivity, high hardness and good corrosion resistance. Along with these properties, low neutron absorption cross section and high recrystallization temperature make TZM particularly useful in nuclear power applications as well as in the aerospace and defense industry. While TZM alloys exhibit excellent strength and toughness, welding of TZM alloys to construct functional structural components is particularly problematic. TZM welds are usually marred by high porosity, a loss of plasticity and brittle failure under loading, and a drastic reduction in joint strength. Joint strength of welded TZM alloy joints drops drastically as shown in Figure 1.4. Chatterjee et al. [39] reported a welded joint yield strength of 41% and 47% to that of the base metal for electron beam welding (EBW) and laser-gas tungsten arc hybrid welding (GTAW) respectively. Stutz et al. [36]

reported a weld strength of 50% to 77% that of the base metal for welds created by EBW. Wang et al. studied EBW butt joints of TZM alloy with different welding speeds [37] and zirconium addition [38] and reported a tensile strength of about 60% that of the base metal. Zhang et al. [40] studied the addition of rhenium in EBW of TZM alloys and reported a joint strength of about 63% that of the base metal. They also reported that the grains in the fusion zone and the heat affected zone were coarse.

Laser welding has many advantages over other conventional welding methods. However, the mechanical performance of welded joints has a lot of room for improvement. Porosity, loss of alloying elements, etc. cause a considerable drop in the material strength at welded joints . Therefore, for currently existing laser welding technologies, a cost effective post processing method is critical for restoration or recovery of material strength at the welded joint.

1.2.4 Laser Shock Peening of Laser Welded Joints

For the improvement of weld strength, post weld treatments such as post weld ageing treatment [41], stress relief annealing heat treatment [42], cold rolling [43] and shot peening [3] have been implemented in the past. However, these methods have inherent limitations: post weld ageing treatment and stress relief annealing have very high processing time, and shot peening has low depth of compressive residual stresses as well as inability of treating all the areas such as internal surfaces of parts with complex geometry. When applied to brittle materials like TZM, shot peening induces undesirable cracking into the material [44]. Laser shock peening (LSP) is a well-established process that imparts beneficial compressive residual stresses to a greater depth into the material, which can induce various benefits such as higher fatigue life and higher stress corrosion resistance. LSP as a post processing technique for welded joints is an area of interest with limited investigations reported in literature. Hatamleh et al. [3, 4] processed friction stir welded (FSW)

joints of Al 7075 and Al 2195 with shot peening and LSP and reported a 13% increase in tensile strength and reduced fatigue crack growth of the LSP processed welded joint. Sakino et al. [5] reported a 5-fold increase in fatigue life of laser welded SM490 steel processed with LSP. Zhang et al. [6] processed laser welded ANSI 304 joints with LSP and reported a 12% improvement in tensile strength of the joint. Chen et al. [7] reported a work hardened depth of up to 1.2mm for laser welded Incoloy 800H processed with LSP along with grain refinement, higher dislocation density, increased hardness, elimination of tensile residual tensile stresses and introduction of compressive residual stresses in the weld zone and heat affected zone. Wang et al. [8] reported improved resistance to stress corrosion cracking and 13% improvement in tensile strength for laser welded Al 7075 processed with LSP. Clauer et al. [9] reported a 7% improvement in yield strength in LSP processed laser welded Al 6061-T6. The mechanisms responsible for these improvements in mechanical performance of welded joints processed by LSP are: (1) conversion of tensile residual stresses (due to welding) into compressive residual stresses, (2) generation of highly dense dislocations due to high strain rate deformations, (3) grain refinement and (4) increased hardness at the surface and up to a certain depth in the material.

For weld strength improvement, the use of LSP as a post processing technique has significant advantages over conventional post processing methods, viz. faster processing times, capability of processing complex weld geometries, in-situ processing of welds in mechanical assemblies. To add to the benefits of processing welded joints with LSP, the use of *w*LSP has the potential of improving the joint strength and increase the stability of compressive residual stresses due to the dislocation pinning effect. However, there is no investigation into the use of *w*LSP as a post processing technique for weld strength enhancement.

1.3 Research Objective

The objective of this study is to assess the potential for a novel dual laser warm laser shock peening as a post processing technique for laser welded joints via simulations and experiments. The specific objectives are as follows:

1. To develop a finite element model for the prediction of indentation depth and residual stresses generated by warm laser shock peening in an oil confinement regime.
2. To develop a novel dual laser warm laser shock peening setup for rapid heating and simultaneous laser shock peening of the target material and validate the finite element model via experiments.
3. To assess the joint strength of laser welded AA6061-T6 and TZM alloys in the Bead-On-Plate and lap weld configurations.
4. To assess the benefits of *w*LSP processing of laser welded joints and investigate the improvement in mechanical performance of the processed welded joints.

1.4 Thesis Outline

In Chapter 2, the finite element modeling of warm laser shock peening is presented. The experimental validation of the finite element model via a novel dual laser warm laser shock peening process is presented. Residual stresses generated due to *w*LSP and rtLSP are presented. In Chapter 3, the *w*LSP processing of laser welded AA6061-T6 and TZM alloy joints is presented. The improvement in joint strength and ductility are presented and the mechanisms for strength enhancement are discussed. Conclusions and recommendations for future work are presented in Chapter 4.

2. FINITE ELEMENT MODELING OF WARM LASER SHOCK PEENING AND EXPERIMENTAL VALIDATION

In this chapter, the finite element modeling of warm laser shock peening (*w*LSP) is presented. A 3-D transient heat transfer model developed by Tian and Shin was utilized to model the laser heating process for achieving desired temperature in the material. A self-closed 1-D hydrodynamic model developed by Wu and Shin [15] was utilized to calculate the plasma pressure history generated for *w*LSP in an oil confinement regime. The finite element analysis methodology used a combined calculation procedure with ABAQUS/EXPLICIT and ABAQUS/STANDARD as shown in Figure 2.1. For AA6061-T6, the Johnson-Cook material model was applied. Actual experimental data was used to define material elastic-plastic behavior for TZM alloy. Experiments were carried out on the base material and the prediction of indentation depths achieved by simulation were successfully validated. The compressive residual stresses predicted by the finite element model demonstrated that the depth and magnitude of compressive residual stresses for *w*LSP are greater than those of rtLSP.

2.1 Laser Heating Model

*w*LSP is a high strain rate plastic deformation process that promotes dynamic precipitation. Therefore, it is critical to ensure that the target material is in the temperature range that promotes dynamic precipitation (400K – 500K). If the material is over heated, there are thermal relaxation and microstructural rearrangement effects that are detrimental to the desired outcome. To locally heat up the target material during *w*LSP experiments, a continuous wave fiber laser with a laser spot size of 500μm (FWHM) and circular Gaussian beam profile was employed. It was essential to understand the correlation between average power of the laser and the peak temperature

achieved in the material. A three dimensional transient heat transfer model for laser heating based on the finite element method developed by Tian and Shin [46] was utilized to predict the temperature in the target material. The model has been utilized previously to predict surface temperatures for a variety of materials such as Ti-6Al-4V, Inconel, Iron, etc.

AA6061-T6 is highly reflective to the 1064nm wavelength light with about 80% of normally incident light reflected off its surface [47]. Therefore, to protect the optical elements of the fiber laser, the angle of incidence of the fiber laser was set to 15° and this was incorporated in the thermal model. The absorptivity and emissivity for rolled aluminum were obtained from the Handbook of Optics [47] and were taken to be 0.20 and 0.06 respectively. Thermal properties of AA6061-T6 and TZM used for the thermal modeling are listed in Table 2.1. To validate the thermal model results, experimental measurements were obtained for parameters listed in Table 2.2. A thermocouple was embedded in the surface of the sample and sealed to the outside environment with thermally insulating cement. The thermocouple was located 2mm from scanning line in a normal direction as shown in Figure 2.1. A NI USB data acquisition system was used to record the temperature measured by the thermocouple. Figure 2.2 shows the validation results for the temperature simulated with the experimentally measured data. The measured values agree very well with the predicted values. With the laser heating model validated, it was utilized to tune laser power in order to achieve desired temperatures in the target material at the laser spot.

Table 2.1. Thermal properties of AA6061-T6 and TZM alloy

Material	Density (kg/m^3)	Thermal Conductivity (W/mK)	Specific Heat (J/kgK)
AA6061-T6 [48]	2700	$164.11+3.58\times10^{-2}T+2.0\times10^{-5}T^2$	$4087.1-17.231T+1.02\times10^{-2}T^2$
TZM [49]	10220	$119-4.46\times10^{-2}T+2.26\times10^{-5}T^2$	$268-3.51\times10^{-2}T+7.27\times10^{-5}T^2$

Table 2.2. Process parameters for validation of laser heating model

Material	Laser Power (W)	Angle of Incidence (deg)	Scanning Speed (mm/s)	Laser beam spot diameter (µm) (FWHM)
Al6061	60	15	1.5	500

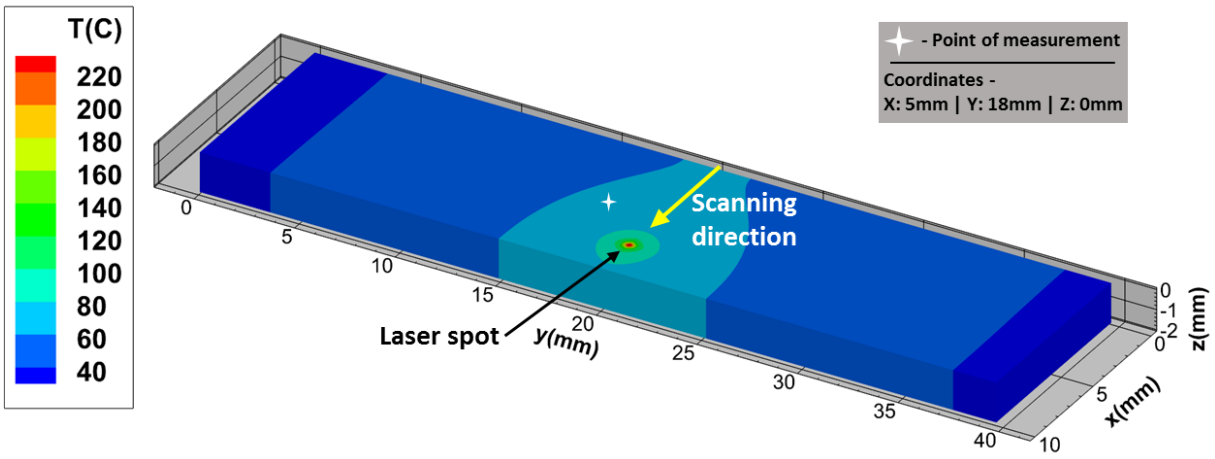

Figure 2.1. Schematic for validation of laser heating model

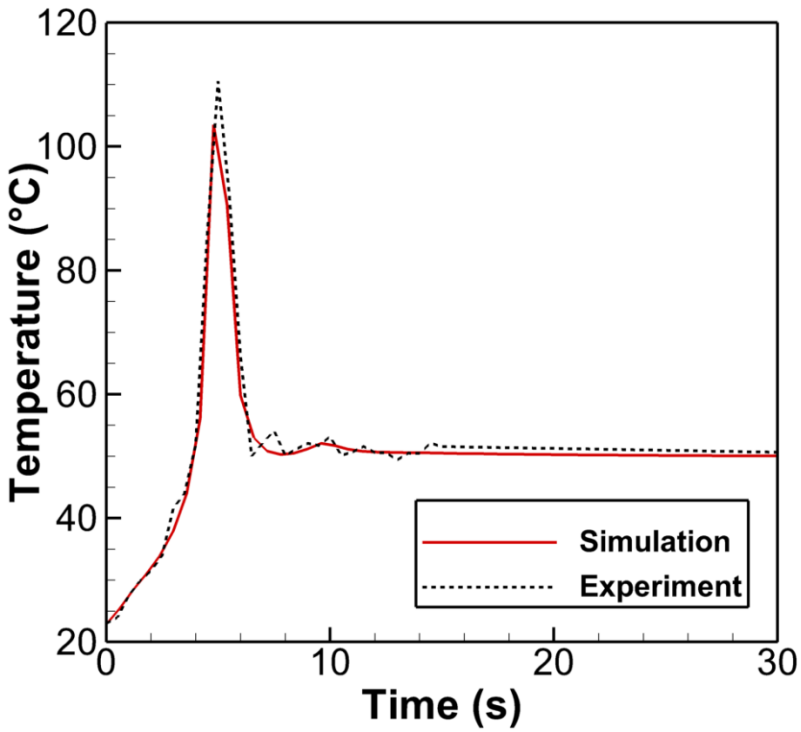

Figure 2.2. Laser heating model validation results

Figure 2.3 shows the temperature profile of the material cross section along the laser scanning line. It can be seen that the peak temperature is achieved up to a depth of 500µm after which the temperature drops. This is beneficial for the current study since (1) compressive residual stresses imparted by LSP become negligible at about 500µm into the depth of the material and (2) the volume fraction of precipitates drops sharply from about 20% at the surface of the material to about 10% at 450µm into the depth of the material [21]. Since *w*LSP is a surface processing phenomenon, it is far more efficient to heat up the material in the work area locally rather than bulk heating of the work-piece.

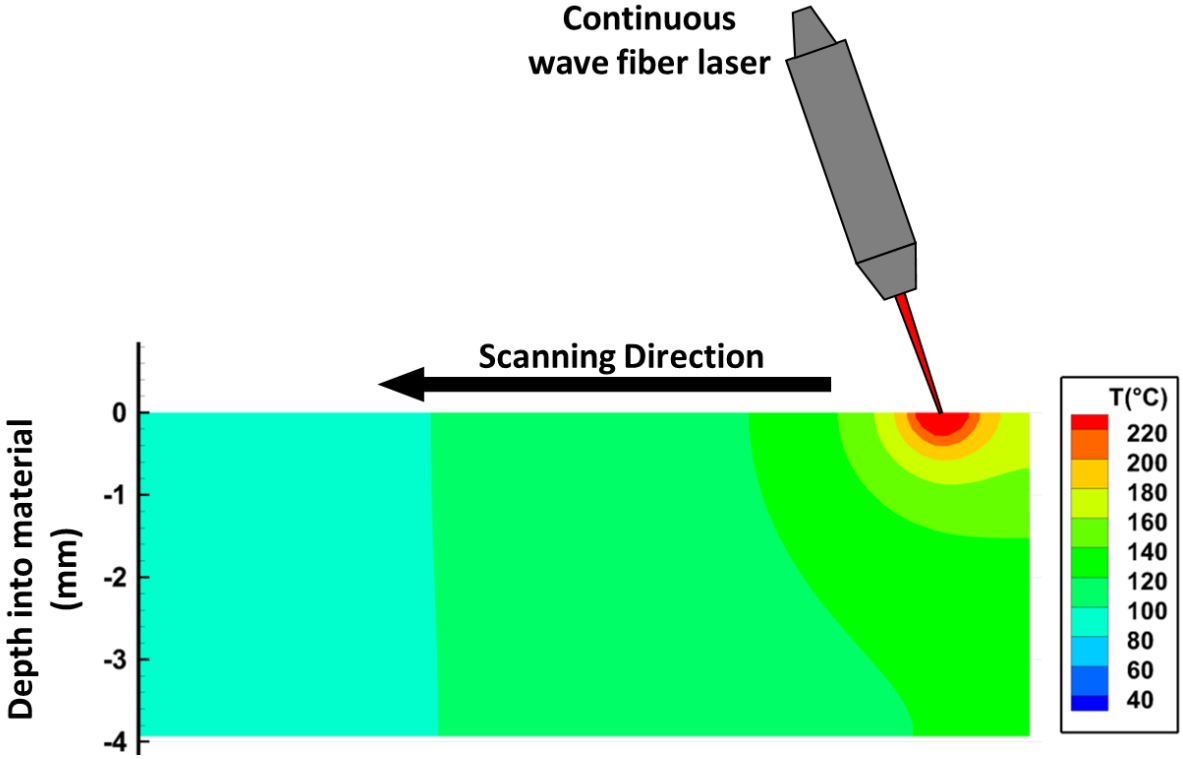

Figure 2.3. In depth temperature profile predicted by the laser heating model

2.2 Plasma Pressure History for *w*LSP Regime

The one-dimensional confined plasma model developed earlier by Wu and Shin [15] was used to predict plasma pressure generated during *w*LSP in an oil confinement regime. Wu and Shin

[50] stated that the two dimensional plasma expansion effects were important only for very small laser beam diameters and that the one-dimensional assumption was valid for beam diameters equal to or larger than 300μm. In this study, since the beam diameter used is 500μm, the one dimensional model is sufficient to describe plasma behavior under oil confinement.

In the one dimensional confined plasma model, the major properties of silicone oil and aluminum were used to compute the ionization of the oil vapor and the coating layer which causes confined plasma to form. In this model, the reflectivity at the oil-plasma interface was calculated through the Drude model. The Saha equations were used for silicon, hydrogen and oxygen, which are the primary elements in the silicone oil. The model considered most important physical processes of laser shock peening, including laser ablation of the coating layer, oil evaporation, plasma ionization and expansion, energy loss of plasma through radiation and electron conduction, laser absorption by plasma, reflection of the laser beam at the air-oil interface and oil-plasma interface, etc. The one dimensional model was validated successfully against experimental results in literature [15] and the description of the model as well as the code used in this part of the work is taken from [15].

Figure 2.4 shows the plasma pressure predicted by this model for the water confinement regime (rtLSP) and the oil confinement regime (*w*LSP). The laser pulse width is 6ns FWHM with a power intensity of 7 GW/cm^2. For rtLSP, the transparent overlay is water, the coating layer is 50μm black paint and the target material is AA6061-T6. For wLSP, the transparent overlay is silicone oil, the coating layer is 50μm aluminum foil and the target material is AA6061-T6. The plasma history for wLSP shows that in an oil confinement regime, the plasma pressure duration is longer than rtLSP.

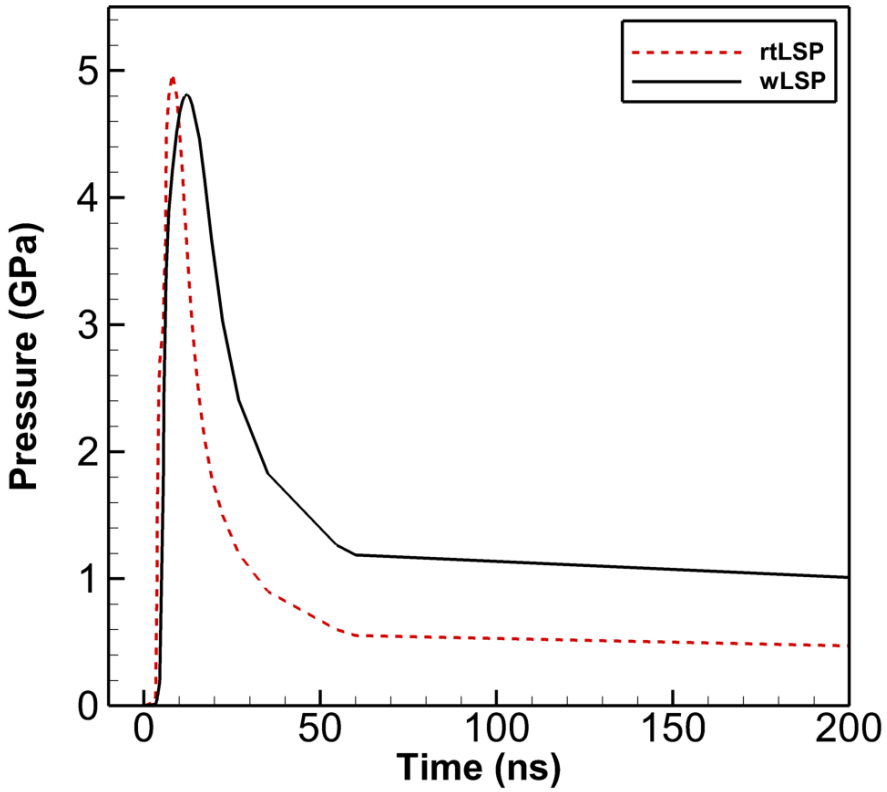

Figure 2.4. Plasma pressure history for LSP and wLSP of AA6061-T6 (laser wavelength 1064nm, FWHM 6ns, 50μm black paint [LSP] / 50μm Al foil [wLSP])

2.3 3-D Finite Element Modeling

2.3.1 Material Modeling

The dynamic behavior of the target material plays a critical role in the development of residual stresses. When a high pressure shockwave is traveling through the material, plastic deformation occurs when the magnitude of the shock wave is greater than the dynamic yield strength of the material. The dynamic yield strength of the material is significantly increased due to strain rate hardening and the work hardening effect. Therefore, the use of an appropriate constitutive plasticity model is essential for capturing the dynamic behavior of the target material in order to simulate the residual stresses in the material.

2.3.1.1 Aluminum 6061

The dynamic response of AA6061-T6 was described by the Johnson-Cook constitutive model [51] represented by,

$$\sigma = (A + B\varepsilon^n)\left(1 + C\ln\left(\frac{\dot{\varepsilon}}{\dot{\varepsilon}_0}\right)\right)\left(1 - \left(\frac{T - T_{ref}}{T_m - T_{ref}}\right)^m\right) \quad (1)$$

with the material properties listed in Table 2.3 and Johnson-Cook constitutive model parameters listed in Table 2.4.

Table 2.3. Material properties of AA6061-T6 [52]

Material	E (GPa)	G (GPa)	ν	ρ (kg/m^3)	T_m (°C)	Thermal expansion (10^{-6}/°C)	Thermal conductivity (W/m K)	Specific heat (J/kg K)
AA6061-T6	68.9	26	0.33	2700	582	23.6	167	896

Table 2.4. Johnson-Cook constitutive model parameters of AA6061-T6 [51]

Material	A (MPa)	B (MPa)	n	C	M	T_{ref} (°C)	T_m (°C)	$\dot{\varepsilon}_0$ (1/s)
AA6061-T6	324.0	114.0	0.42	0.002	1.34	25	582	1

2.3.1.2 TZM alloy

The hot rolled TZM alloy sheets used in this study had material properties listed in Table 2.5. TZM alloys are scarcely studied in literature and hence a constitutive plasticity model was not available. Therefore, the material elastic plastic behavior determined experimentally was mapped using the classic metal plasticity model with isotropic hardening behavior based on von Mises yield surfaces. The elastic and plastic behavior of the material was mapped using experimental

tensile testing data. Figure 2.5 shows the true stress vs true strain data obtained for as received TZM alloy.

Table 2.5. Material properties of TZM alloy

Material	E (GPa)	ν	ρ (kg/m^3)
TZM	324.0	0.42	10220

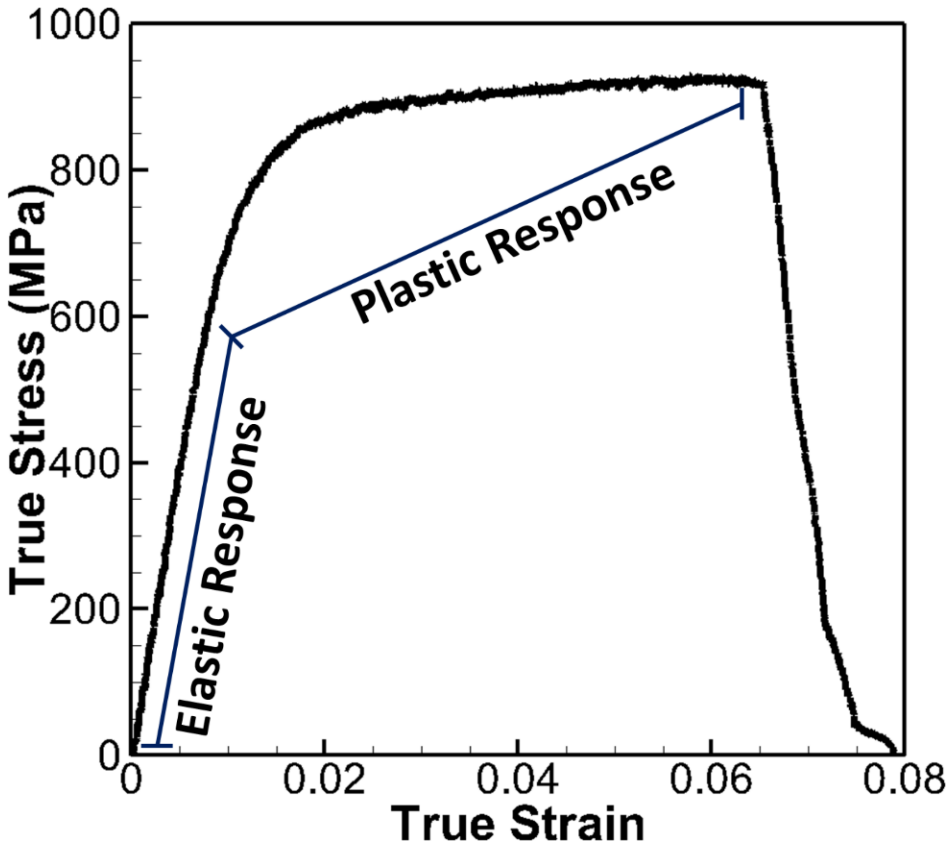

Figure 2.5. Stress-Strain curve obtained from experimental data used for material modeling of TZM alloy

2.3.2 Finite Element Model

A 3-D finite element model (FEM) has been developed to calculate the shock wave propagation through the target material and the residual stresses in the material by using the

confined plasma pressure as input was used as the . The pulsed laser used in this study has a flat-top beam profile; therefore, the plasma pressure was modeled as a distributed pressure over the beam diameter controlled by the user subroutine VDLOAD as shown in Figure 2.6. Encastre boundary conditions were applied to the bottom surface of the material. The coating layer used in this study was 50μm thick Al 1100 foil. The mechanical and physical properties of the coating layer were obtained from literature [53, 54]. Coupling of the coating layer and the target material at the interface was accomplished with the TIE constraint in ABAQUS. The TIE constraint ensures that the displacement of nodes closest to the interface in the target material will be kept the same as that of the nodes in the coating layer, closest to the interface.

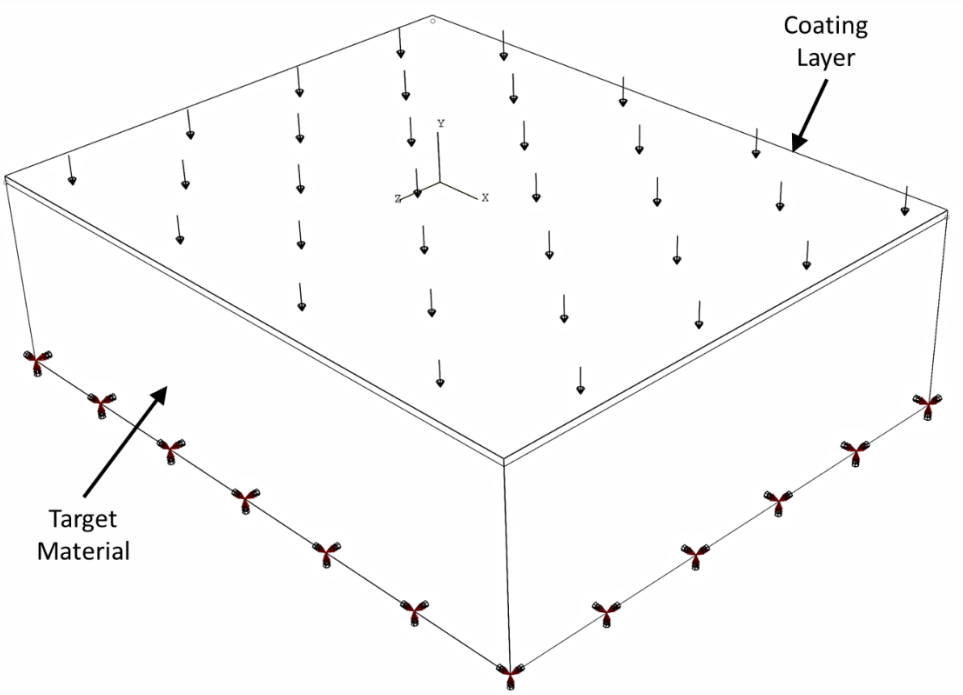

Figure 2.6. 3-D Finite Element Model

2.3.3 Calculation Procedure

The FEM calculation procedure for multitrack wLSP is shown in Figure 2.7. A computationally efficient calculation methodology is used, which combines ABAQUS/EXPLICIT

to calculate the shock wave propagation and ABAQUS/STANDARD to compute the residual stresses [12].

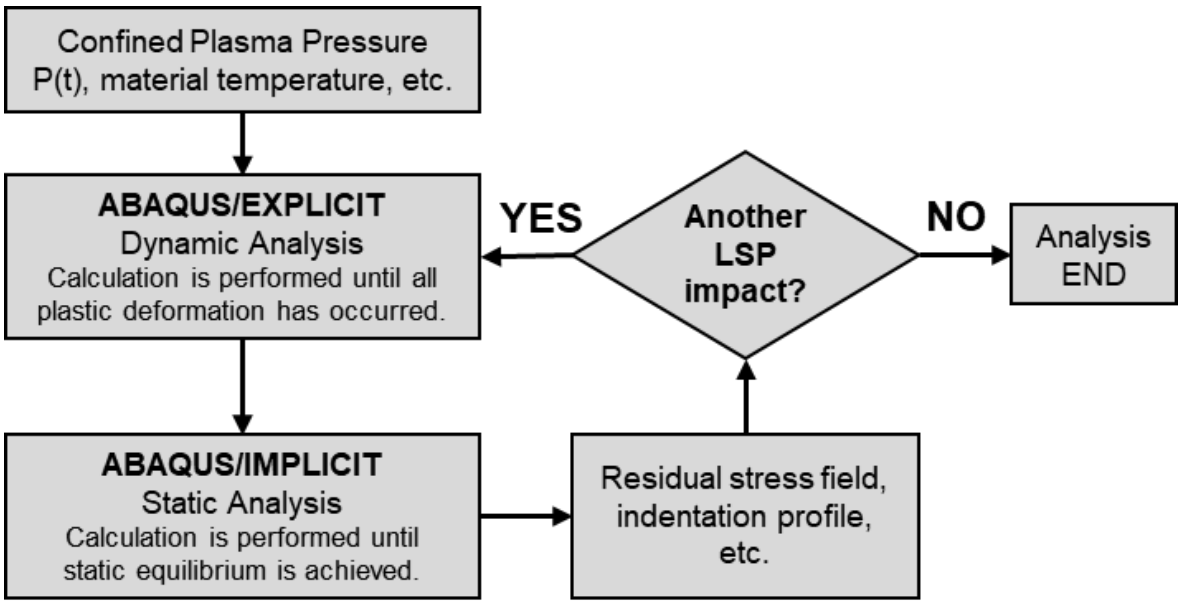

Figure 2.7. FEM calculation procedure [19]

2.4 Experimental Validation

2.4.1 Setup and methods

The experimental setup that was used for modeling validation as well as *w*LSP processing of welded joints is shown in Figure 2.8. An Nd-YAG laser (Continuum Surelite III-10) beam with a wavelength of 1064nm and the pulse duration of 6ns was focused onto the top surface of the workpiece to perform LSP, after passing through a half wave plate, thin film polarizer, three high reflecting mirrors and a focusing lens. The focused laser beam diameter on the surface of the workpiece can be changed by varying the distance between the workpiece and the focusing lens. The beam profile of the pulsed laser is top-flat and shown in Figure 2.9. With this setup, the power density of the pulsed laser can be easily adjusted by finely adjusting the half wave plate orientation. A secondary continuous wave fiber laser (IPG YLR 150/1500 QCW) was focused on the surface of the workpiece such that it coincides with the laser spot of the Nd-YAG laser. The fiber laser

was used to locally heat the workpiece to *w*LSP regime temperatures of 400K-500K. The workpiece was placed in a tank filled with a high temperature silicone fluid (with a flash point of 590K) to produce a fluid confinement regime.

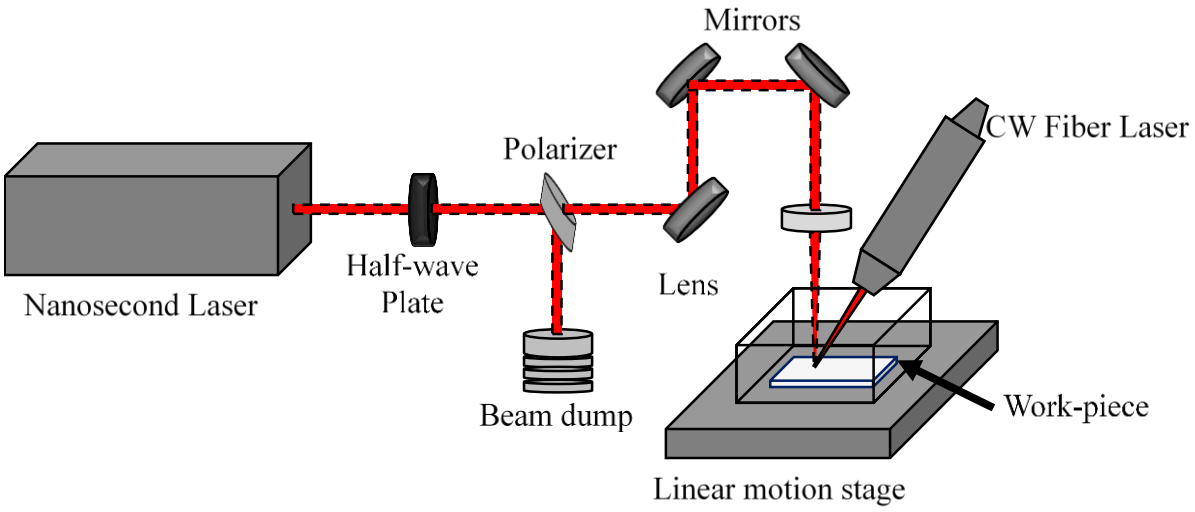

Figure 2.8. Schematic diagram of experimental setup for wLSP

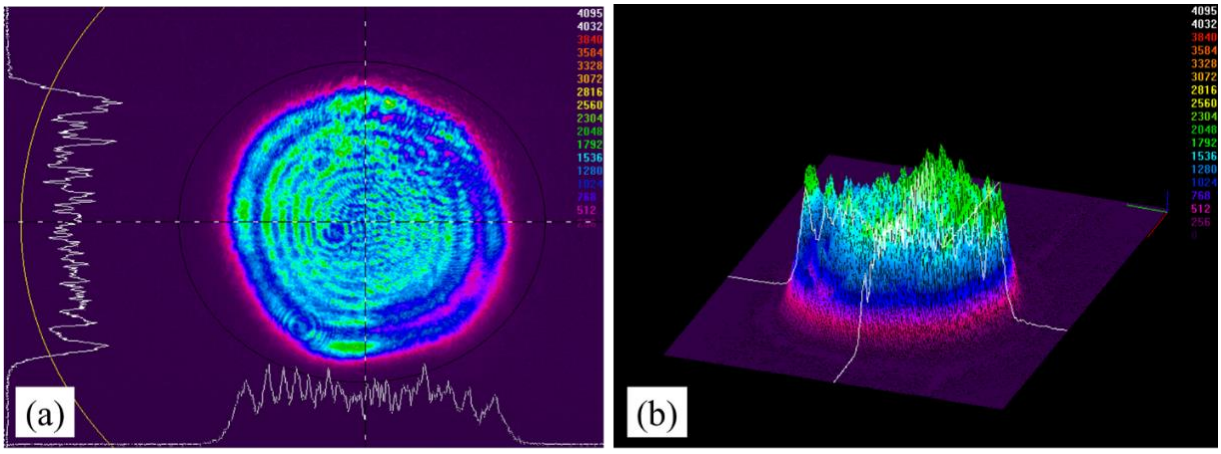

Figure 2.9. Measured beam profile (a) 2-D (b) 3-D [18]

The samples used in the experimental validation of the finite element model were as received rolled sheet of AA6061-T6 with a thickness of 2 mm and hot rolled TZM alloy sheet with a thickness of 1 mm. Parameters for single shot and single track overlap peening experiments are listed in Table 2.6.

Table 2.6. Processing parameters for LSP experiments

	Single Shot LSP		Single track overlap LSP
Processing Condition	rtLSP	wLSP	wLSP
Material	AA6061-T6, TZM	AA6061-T6, TZM	AA6061-T6
Laser Power Intensity (GW/cm^2)	7	7	3, 5, 7
Coating Layer	Black paint	Al foil	Al foil
Transparent overlay	Water	Silicone oil	Silicone oil
Overlap ratio	-	-	50%
Material temperature (K)	~296	~500	~500

2.4.2 Results and Discussions

2.4.2.1 Indentation Depth

As the confined plasma model and the 3-D finite element model have been validated extensively by Wu and Shin [19] and Cao and Shin [18], measuring the indentation depth for experimental *w*LSP samples and comparing it with simulation results was sufficient for validation of the modeling work. Indentation profiles of *w*LSP processed samples were measured by a Bruker Contour GT-K 3-D optical profiler. Figure 2.10 shows the surface profile measurements for single shot and single track overlap *w*LSP processing of AA6061-T6. For single shot LSP, the indentation depths measured for 5 shots were compared with simulation values. Experimental measurements are in good agreement with the simulated indentation depths as can be seen from Figure 2.11. Average indentation depths measured for *w*LSP processing using the laser power densities listed in Table 2.6 are shown in Figure 2.12 and agree well with simulated indentation depth values.

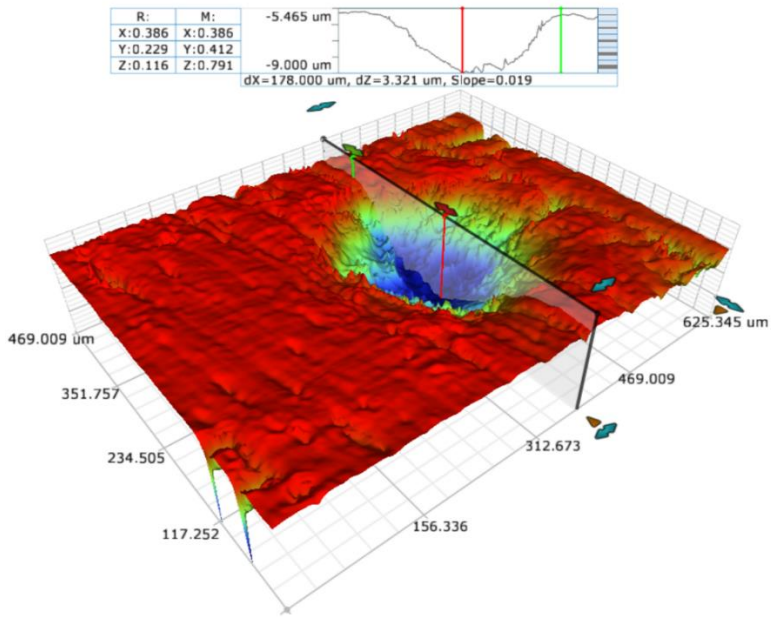

(a)

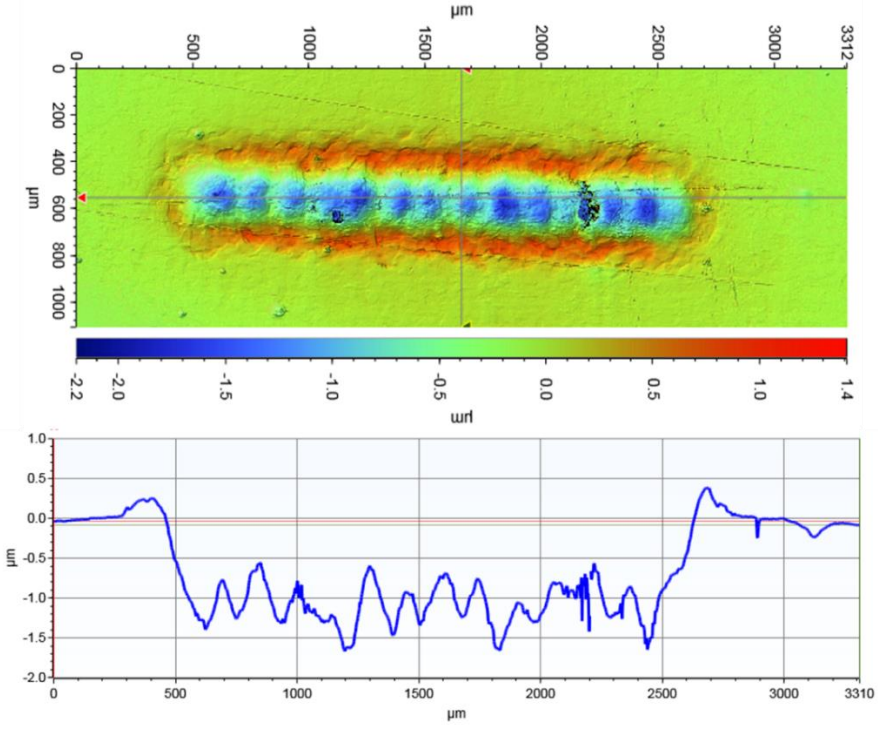

(b)

Figure 2.10. 3-D optical profile measurements for (a) single shot and (b) single track overlap wLSP processing of AA6061-T6

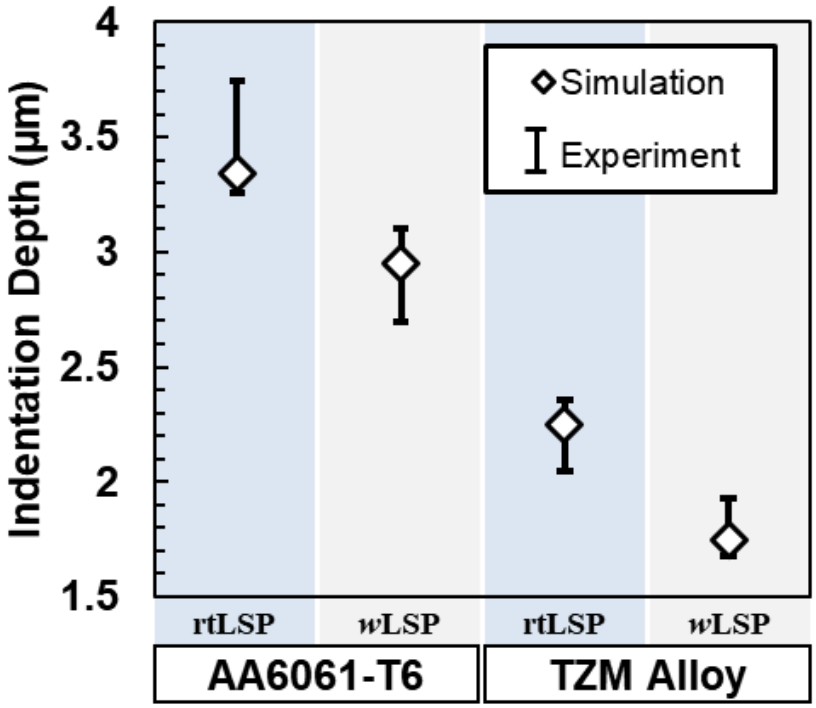

Figure 2.11. Indentation depths measured for simulation and experiments of single shot LSP processing with laser power intensity of 7 GW/cm2

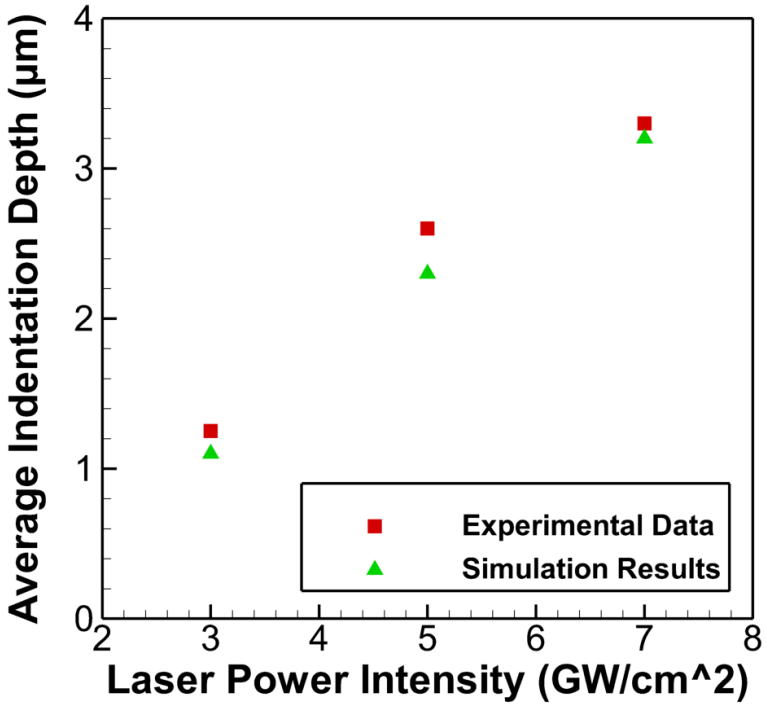

Figure 2.12. Comparison of average indentation depth under different laser power intensities for single track overlap wLSP processing

2.4.2.2 Residual Stresses

As mentioned in Section 2.4.2.1, the confined plasma model and 3-D finite element model have been extensively validated for indentation depth and residual stresses. Since the maximum indentation depth was achieved for a laser power intensity of 7 GW/cm^2, it was used as the processing power for further experiments and simulations. Once the indentation depths were validated, the residual stresses in the depth of the material predicted for *w*LSP were compared with rtLSP. Figure 2.13 shows the residual stresses predicted for rtLSP and *w*LSP processing of AA6061-T6 and TZM alloy. From the predictions it can be seen that for *w*LSP, the compressive residual stresses induced in the material are greater in magnitude and depth into the material than rtLSP. The warm temperature shot peening of AISI 4140, carried out by Menig et al. [55], also reported a similar deeper and greater magnitude of compressive residual stresses. The elevated temperature of the target materials enables a deeper travel of the incident shockwave, thereby plastically deforming a larger region. It should be noted here that while deeper plastic working is a virtue of the elevated temperature, increasing the processing temperature results in recovery of residual stresses, which is counterproductive to the purpose of *w*LSP processing. The processing temperature range for this study was obtained from various published works [21, 22]. The greater and deeper compressive residual stresses predicted by this process combined with the dislocation pinning effect [56] would result in enhanced mechanical properties of materials processed with the dual-laser *w*LSP processing technique.

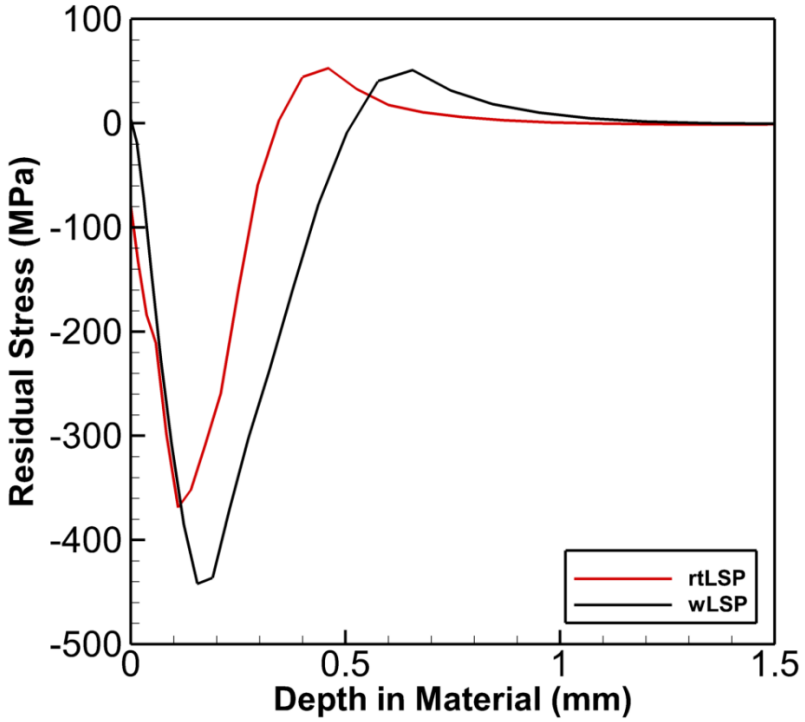

(a)

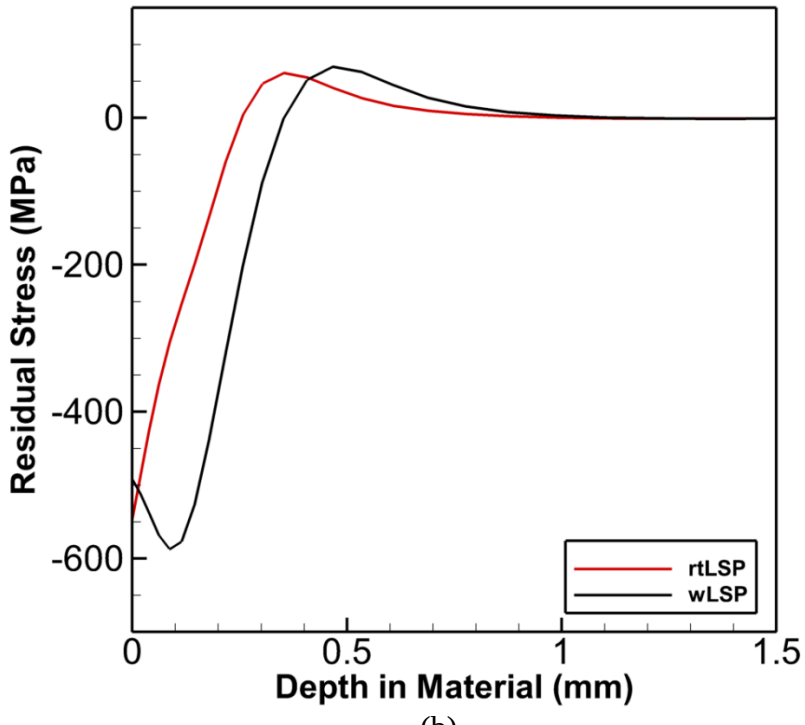

(b)

Figure 2.13. Residual stress prediction for (a) AA6061-T6 and (b) TZM alloy

3. WARM LASER SHOCK PEENING OF LASER WELDED AA6061-T6 AND TZM ALLOY

In this chapter, the effect of warm laser shock peening on laser welded AA6061-T6 and TZM alloy joints is presented. Experimental methodologies for laser welding, warm laser shock peening, mechanical testing and material characterization are presented in Section 3.1. The key welding parameters of the welded joints used in this study are listed in Table 3.4. To evaluate the benefits of *w*LSP over rtLSP, mechanical testing of joints processed by these methods was carried out. Mechanical testing results and failure mode analyses of *w*LSP processed samples are presented in Section 3.2. Lap welded joints when loaded under tensile shear conditions have complex stress profiles. To understand the stress concentration regions in tensile shear testing of lap welded joints, finite element analysis was carried out. Microhardness based weld region strength values were used in the material modeling of the weld region. The failure modes predicted by actual testing of lap welded joints are better explained by the stress profile predicted by the finite element model.

3.1 Experimental Methodology

3.1.1 Laser Welding

Rolled sheets of AA6061-T6 with a thickness of 1-2 mm and hot rolled TZM alloy sheets with a thickness of 0.5-1 mm were used in this study. Table 3.1 lists the composition of AA6061-T6 while Table 3.2 lists the composition of TZM alloy. Table 3.3 lists the thickness of materials used for the different welding configurations. Prior to welding, the samples were ground using sandpapers to remove rough ridges and then cleaned with acetone to remove the oxide layer and any residual grease.

Table 3.1. Chemical composition of the as-received AA6061-T6 alloy

Element	Si	Fe	Cu	Mn	Mg	Cr	Zn	Ti	Other	Al
Content %	0.69	0.43	0.22	0.13	0.87	0.16	0.04	0.02	0.03	Rem.

Table 3.2. Chemical composition of the as-received TZM alloy

Element	Fe	Ni	Si	Ti	Zr	C	N	O	Mo
Content %	0.0007	0.0005	<0.002	0.47	0.087	0.022	0.003	0.042	Rem.

Table 3.3. Material thickness for various welding configurations

Material	Welding configuration	Material Thickness
AA6061-T6	Overlap weld	1 mm
	BOP weld	2 mm
TZM alloy	Overlap weld	0.5 mm
	BOP weld	1 mm

The key welding parameters such as interface gap, laser power, welding speed, shielding gas etc. and experimental setup were obtained from Pellone et. al. [35] and Ning et al. [57]. Welding experiments were performed with an IPG YLS-1000 fiber laser (wavelength: 1077nm) with a laser spot diameter of 240 μm and a circular Gaussian beam profile. The maximum power of the laser is 1000 W. During welding, the laser beam was inclined by 10° to protect the laser beam delivery optics from the induced plasma and splatter. Shim stocks were used to introduce and maintain the interface gap while clamping workpieces on the work surface. Argon or Helium was used as the shielding gas for the top surface via side and coaxial nozzles and for the bottom surface via another nozzle. Lap welding experiments were conducted in keyhole welding mode.

For BOP welding, the setup is the same as that in lap welding except for the setup of the workpieces. The schematic diagram of the laser welding system is shown in Figure 3.1. Welding parameters for AA6061-T6 and TZM alloys are listed in Table 3.4.

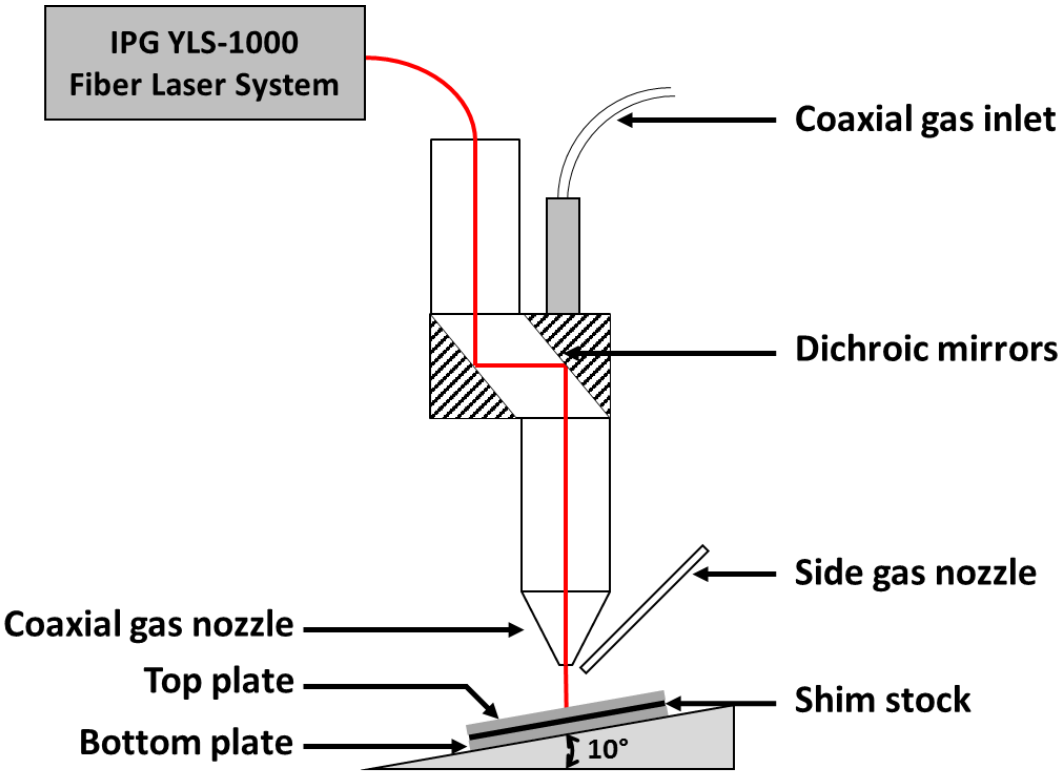

Figure 3.1. Schematic of laser welding system

Table 3.4. Welding parameters for lap and BOP welds

Material	Plate Thickness (mm)	Joint Type	Laser Power (W)	Welding Speed (m/min)	Interface gap (mm)	Shielding gas type
AA6061-T6	1	Lap	1000	1.4	0.038	He
	2	BOP	1000	1.4	-	He
TZM	0.5	Lap	850	1	0.09	Ar
	1	BOP	1000	0.5	-	Ar

3.1.2 Warm Laser Shock Peening

The same experimental setup shown in Figure 2.9 was used in this study. Prior to *w*LSP processing, welded samples were first machined to dimensions required for tensile-shear and standard tensile tests per ASTM E8 standards. To prepare samples, a Flow Mach 2 2020c water jet machine was utilized. Dimensions of samples and peening surfaces are shown in Figure 3.2.

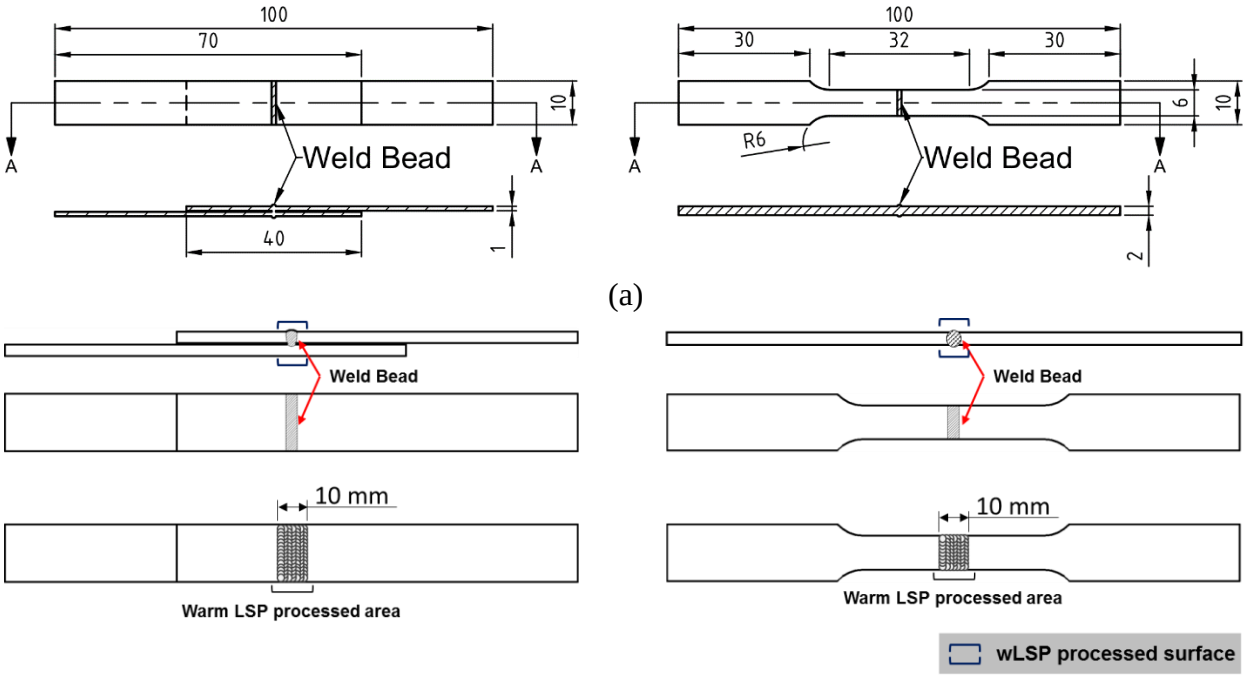

Figure 3.2. (a) Dimensions and (b) processing surfaces for wLSP of welded joints

3.1.3 Mechanical Testing

Tensile shear tests for lap welded joints and standard tensile tests for BOP welded joints were carried out on an MTS 858 Mini Bionix machine shown in Figure 3.3. The testing speed was determined by a constant displacement rate of 0.5 mm/min for each sample. The mechanical testing was carried out per ASTM E8 standard.

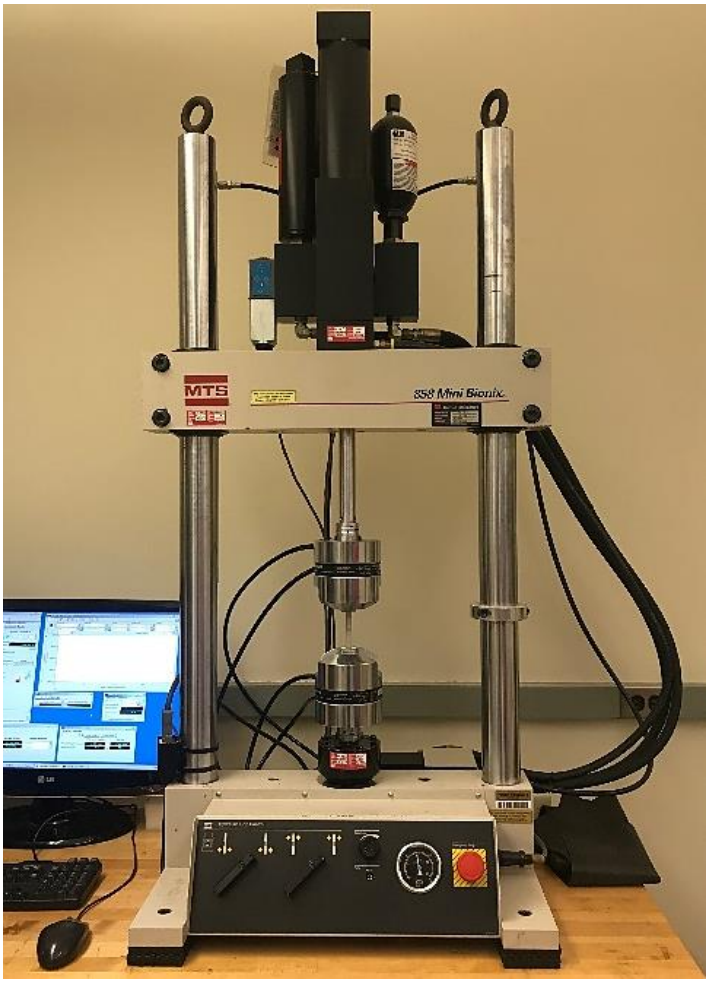

Figure 3.3. MTS 858 Mini Bionix machine used for mechanical testing

3.1.4 Material Characterization

To characterize the failure modes and microhardness of samples, untested and tested samples were mounted using compression hot mounting in Bakelite. Mounted samples were polished with abrasive papers of 180, 240, 320, 400, 600, 800, 1200 grits. Final polishing was carried out with an oil suspension of 6µm and 3µm diamond paste and with colloidal silica water suspension of 0.5µm on a polishing cloth wheel. Polished AA6061-T6 samples were etched with a NaOH etchant and TZM samples were etched with an etchant comprising of 3mL H_2O, 5mL HNO_3, and 2mL H_2SO_4. A Nikon Eclipse LV150 optical microscope was used to observe the fracture morphology

and microstructure of the samples. Microhardness measurements were carried out using a LECO LM247AT microhardness tester and AMH43 analysis software.

3.2 Results

3.2.1 Evaluation of *w*LSP benefits over rtLSP for welded joints

The effects of *w*LSP on materials and its comparison with rtLSP has been reported in literature. However, there are no reports of rtLSP and wLSP processing of welded joints. Therefore, to evaluate the benefits of wLSP processing of welded joints over rtLSP, BOP welded joints were processed with rtLSP and wLSP using parameters listed in Table 3.5. Figure 3.4 shows BOP samples as welded and then processed with *w*LSP on the top and bottom surfaces.

Table 3.5. Parameters for rtLSP and wLSP processing of BOP samples

Type of LSP	Coating Layer	Confinement Layer	Workpiece Temperature (K)	Laser Power Density (GW/cm^2)	Peening Overlap Ratio
Room Temperature LSP (rtLSP)	50µm thick Black Paint	Water	300	7	50%
Warm LSP (*w*LSP)	50µm thick Aluminum Foil	High temperature silicone oil	425-500	7	50%

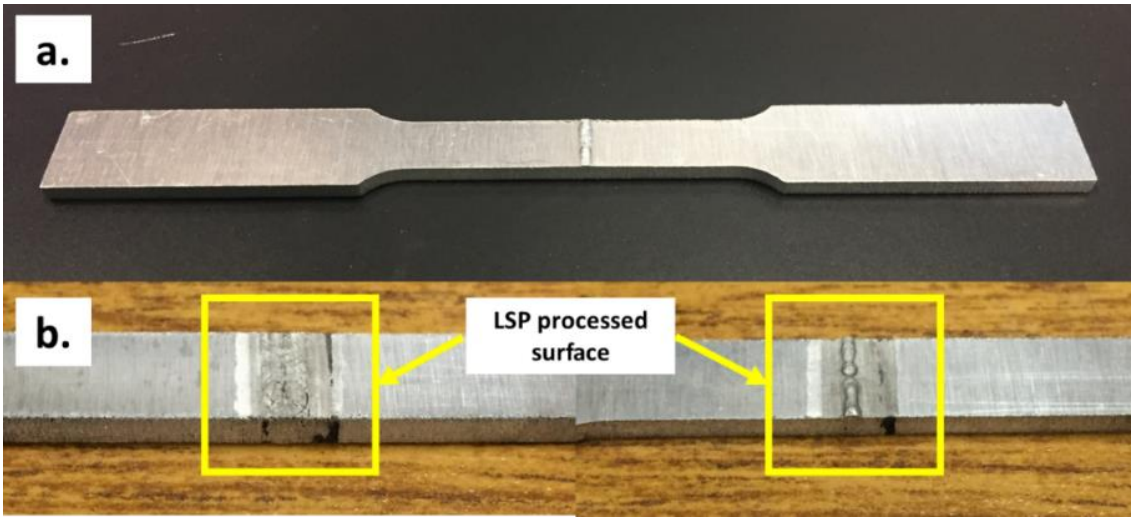

Figure 3.4. BOP sample processed with wLSP

Tensile testing of the LSP processed samples demonstrated an improvement in strength of joints over as-welded samples. Figure 3.5 shows the tensile strength and elongation to failure for BOP samples for three processing conditions viz. 'as-welded', 'as-welded + rtLSP' and 'as-welded + *w*LSP'. It is clear that *w*LSP processed samples show significant improvement in tensile strength of joint than rtLSP. Samples processed with *w*LSP also exhibit improved ductility than rtLSP. The deeper compressive residual stresses, along with the dislocation pinning effect (discussed in Section 3.3) contribute to the improvement in strength while retaining and improving ductility. Due to the significant advantage posed by *w*LSP processing in improving mechanical performance of welded joints, all BOP and overlap welded samples were processed with *w*LSP.

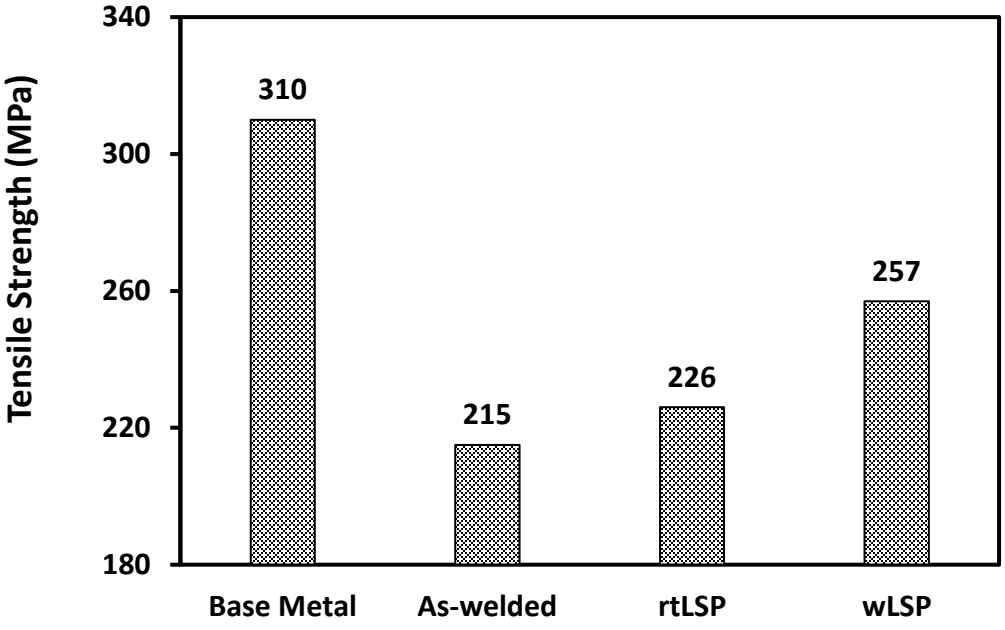

(a)

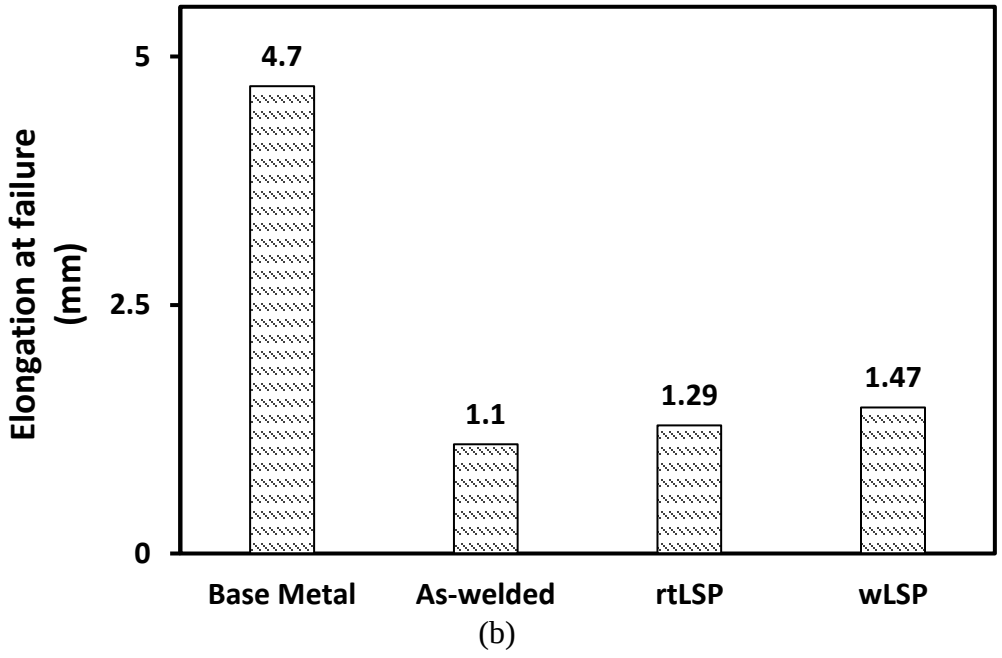

(b)

Figure 3.5.(a) Tensile strength and (b) elongation to failure for welded samples processed with rtLSP and wLSP

3.2.2 Effect of *w*LSP on AA6061-T6 BOP welded joints

Load vs displacement curves for tensile testing of AA6061-T6 BOP welded joints processed with *w*LSP are shown in Figure 3.6. The *w*LSP processed samples demonstrated higher loads carried than as-welded samples. There is also notable ductility improvement in the *w*LSP processed joints. As shown in Figure 3.5 the *w*LSP processed BOP welded joints demonstrated an improvement of 20% in the weld strength and about 34% improvement in ductility of the joint. Figure 3.7 shows the failure morphology of the tested joints. The failure mode is distinctly ductile with typical necking of the rupture region visible close to the crack. For 'As-Welded' samples, the ductile rupture originated from the bottom of the weld with columnar grains having lower hardness as shown in Figure 3.8. The width of coarse columnar grains in the fusion zone, as shown by the light blue arrows, for untreated samples is larger than that of *w*LSP processed samples. In *w*LSP processed samples, the ductile rupture moved slightly towards the center of the fusion zone.

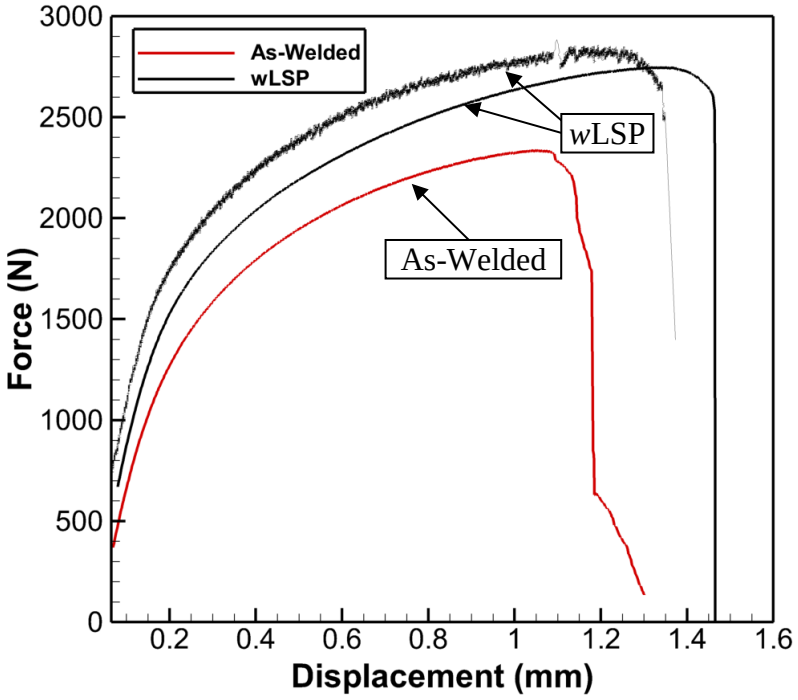

Figure 3.6. Load vs Displacement curves for tensile testing of AA6061-T6 BOP welded joints

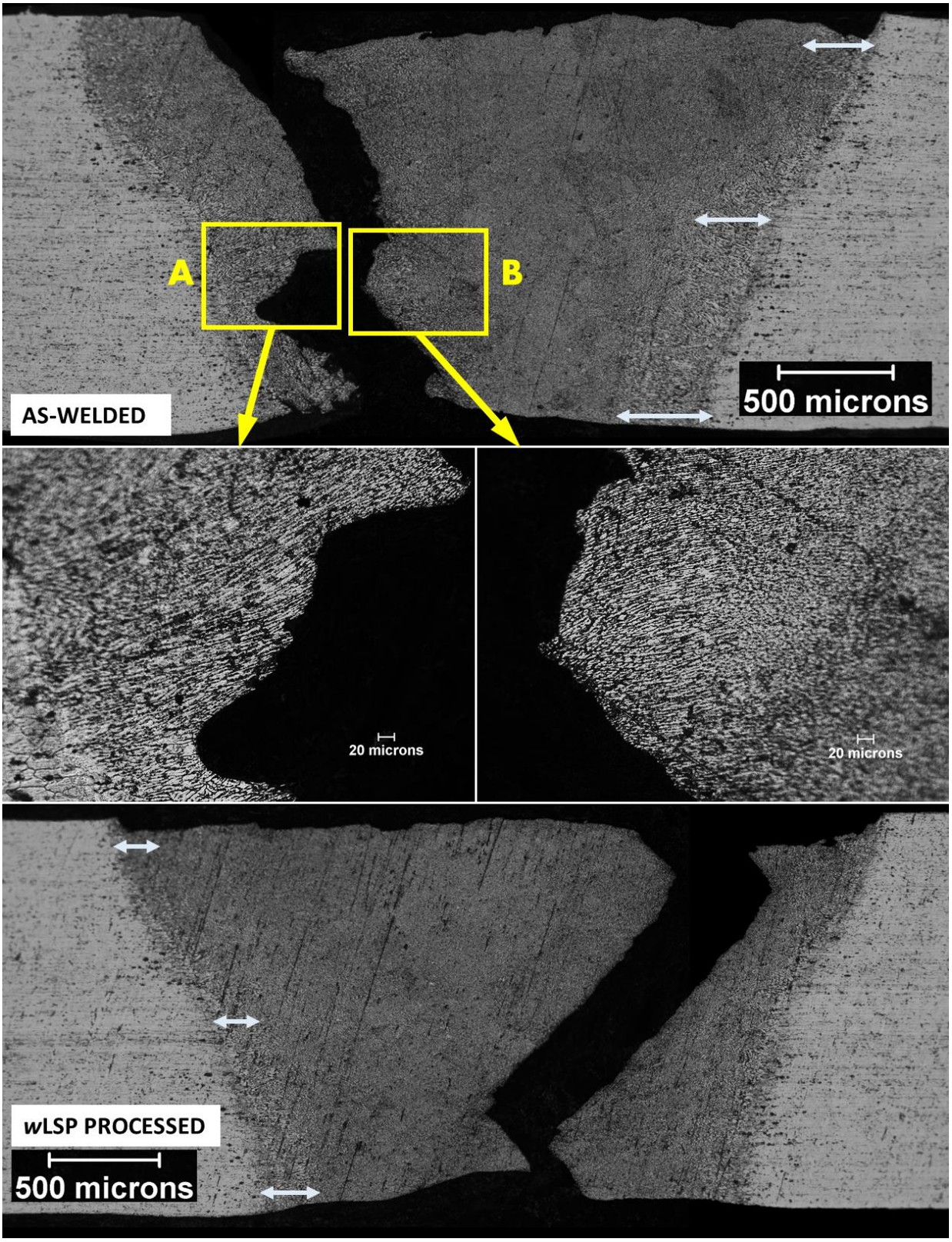

Figure 3.7. Failure morphology for as-welded and wLSP processed AA6061-T6 BOP joints

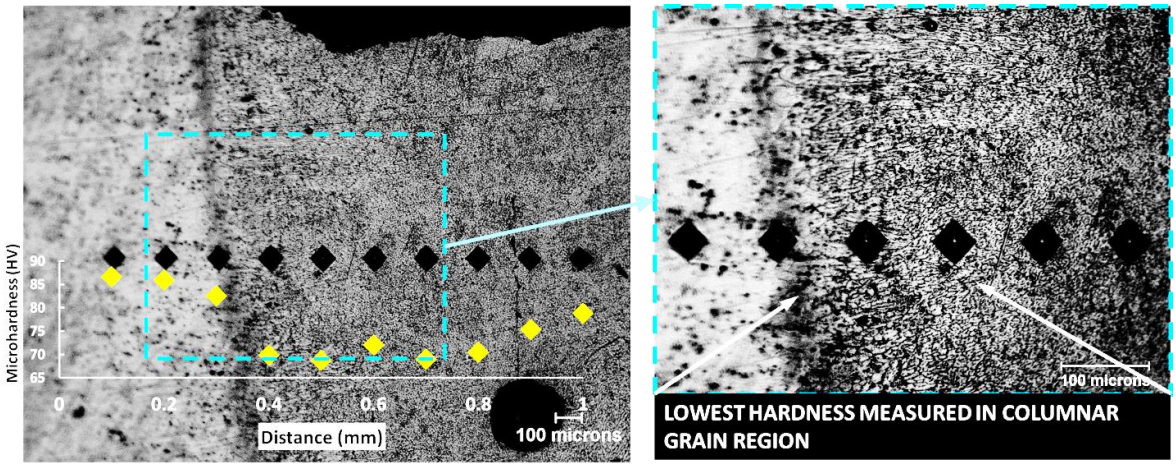

Figure 3.8. Microhardness measured along HAZ and FZ for BOP weld

3.2.3 Effect of *w*LSP on AA6061-T6 lap welded joints

Load vs displacement curves for tensile shear testing of AA6061-T6 lap welded joints processed with *w*LSP are shown in Figure 3.9. The *w*LSP processed joints sustained higher loads than the as-welded samples. Ductility of *w*LSP processed samples improved by about 65%.

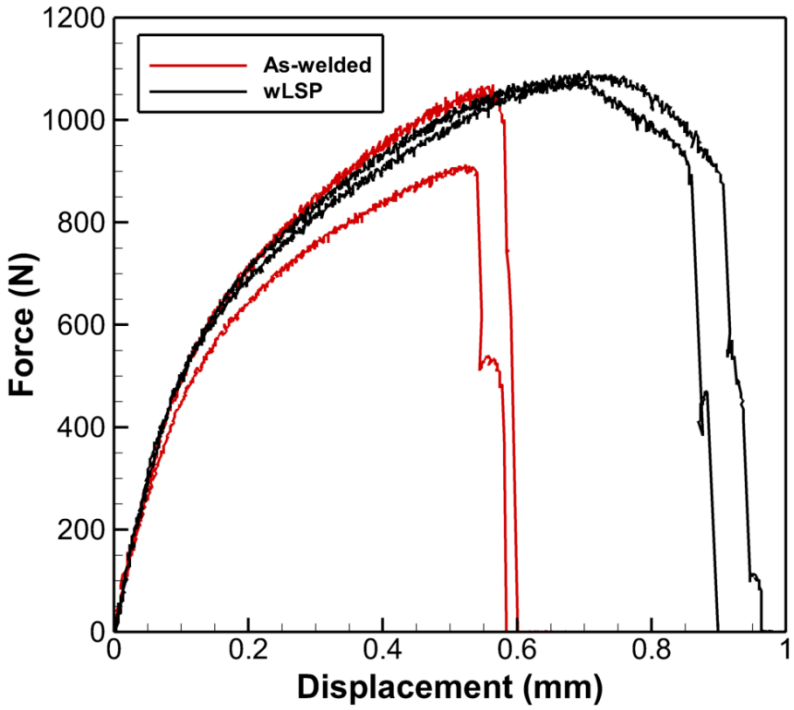

Figure 3.9. Load vs Displacement curves for tensile-shear testing of AA6061-T6 lap welded joints

Although the force applied on the samples in tensile shear testing is uniaxial, the loading of the welded joint is not uniaxial in nature. Therefore, it is necessary to understand the stress concentration regions in the weld zone for better understanding of the failure mechanisms in the samples tested. In order to observe stress concentration regions, a finite element analysis was carried out. The material properties for AA6061-T6 listed in Section 2.3.1.1 were used to represent the material response of the base material. Due to the welding process, the material properties in the fusion zone (FZ) and heat affected zone (HAZ) of the weld change significantly, due to which the material modeling of the base material cannot be applied to these regions. To estimate strength of the FZ and HAZ, microhardness measurements were carried out on the weld region as shown in Figure 3.10. The microhardness measurements were used to compute yield strength and ultimate tensile strength of the FZ and HAZ using the relations defined by Cahoon et al. [58] given by (2) and (3) where *H* is the measured hardness and *m* is the Meyer's coefficient. The Meyer's coefficient was computed with (4) where *n* is the strain hardening exponent (n = 0.042 for AA6061-T6 [59]/ n = 0.202 for TZM alloy [60]). These strength values were used as input for material modeling of the weld region.

$$\sigma_y = \left(\frac{H}{3}\right)(0.1)^{(m-2)} \quad (2)$$

$$\sigma_u = \left(\frac{H}{3}\right)[1-(m-2)]\left[\frac{12.5\,(m-2)}{1-(m-2)}\right]^{(m-2)} \quad (3)$$

$$m = n + 2 \quad (4)$$

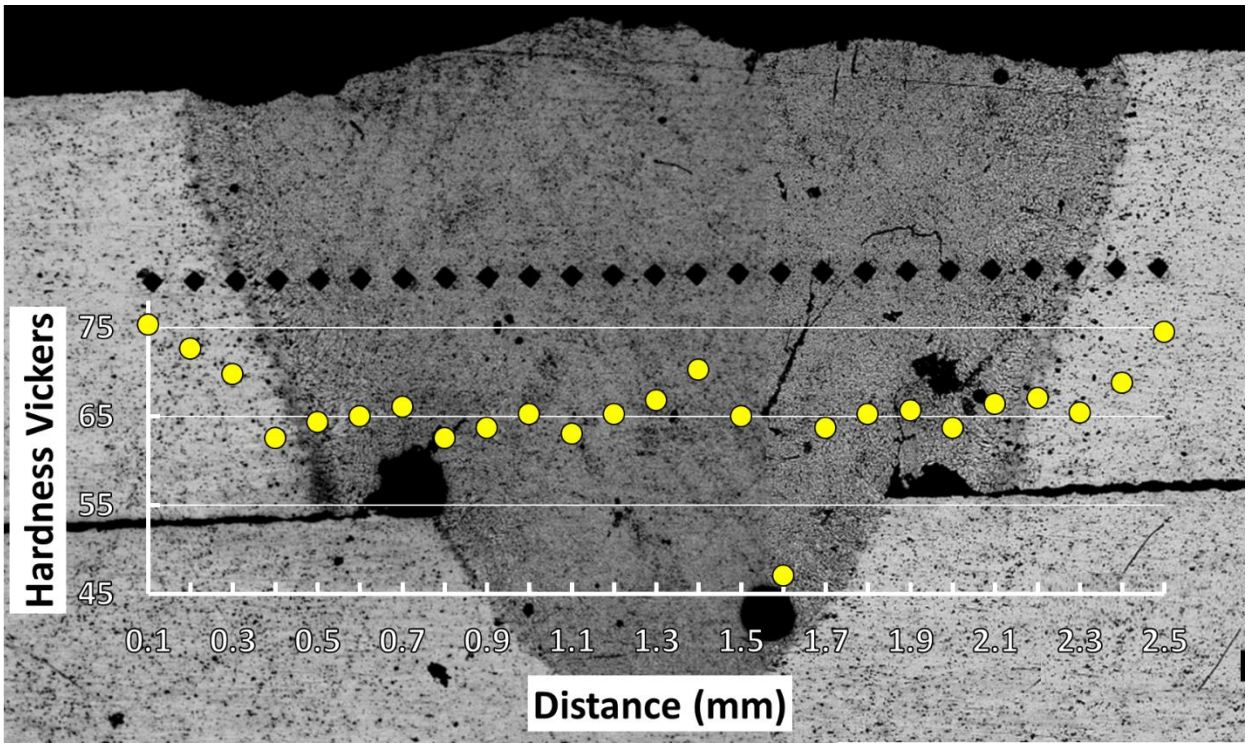

Figure 3.10. Microhardness measurement across weld region for AA6061-T6 lap weld.

The stress concentration regions predicted by the finite element model are shown in Figure 3.11. From the figure, it can be seen that under a tensile shear loading condition, the primary stress concentration propagates from the interface region between the top plate and the bottom plate and then moves along the heat affected zone in the top plate towards the surface of the top plate. A secondary stress concentration can be seen being originating at the interface region at the bottom plate and top plate on the opposite side of the primary stress concentration region.

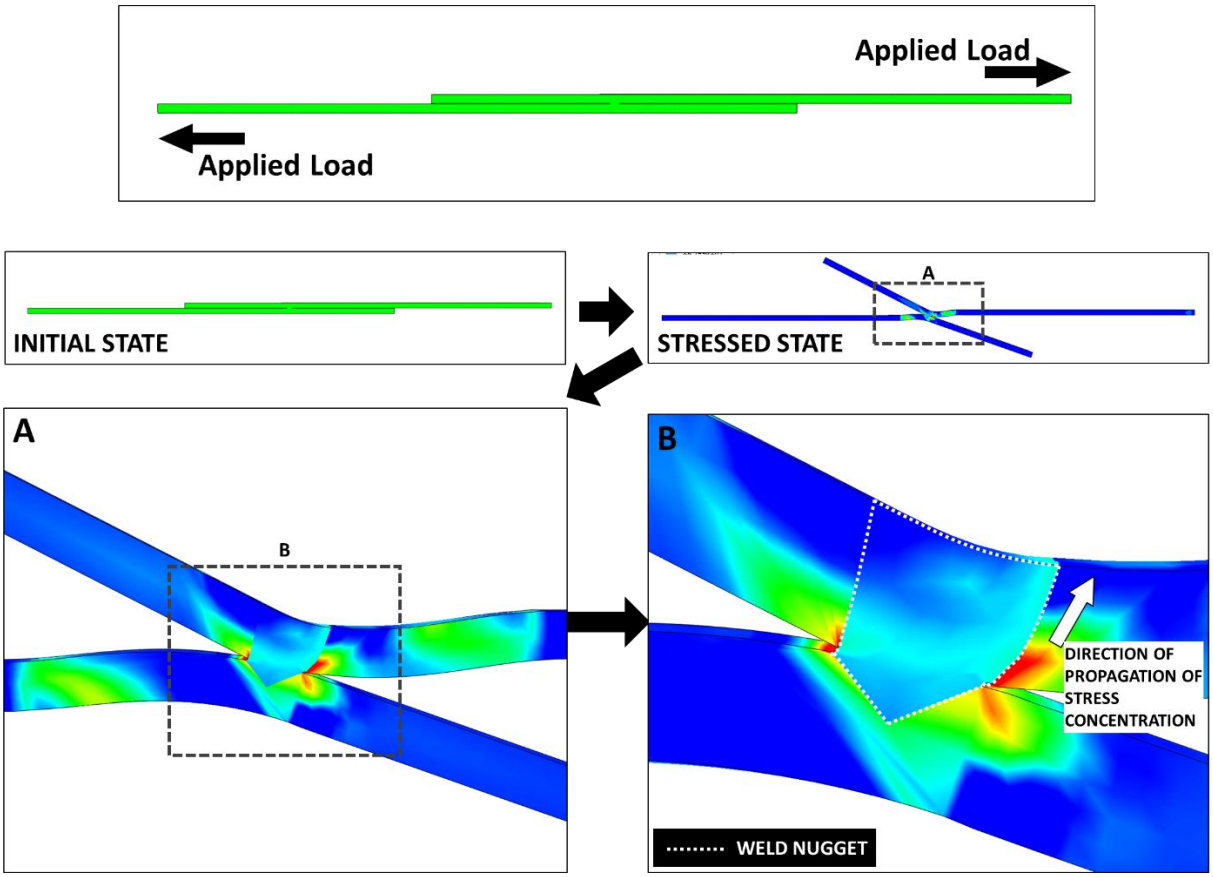

Figure 3.11. Stress concentration regions predicted by finite element modeling of tensile shear loading of AA6061-T6 lap welds

Micrographs of the tensile tested samples are shown in Figure 3.12. From Figure 3.12 (a), it can be seen that the failure regions observed are in good agreement with predicted stress concentration regions. Figure 3.12 (b) shows that for *w*LSP processed samples, the secondary crack initiation and propagation in the bottom plate was restricted. Deformation of the top and bottom plates was lower for *w*LSP processed joints than as-welded joints.

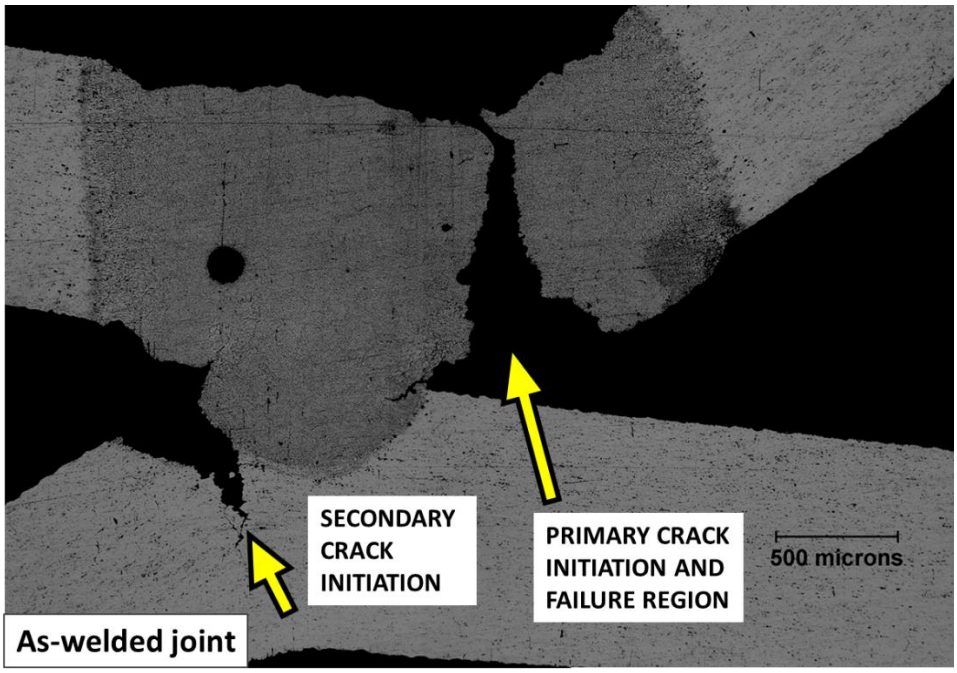

(a)

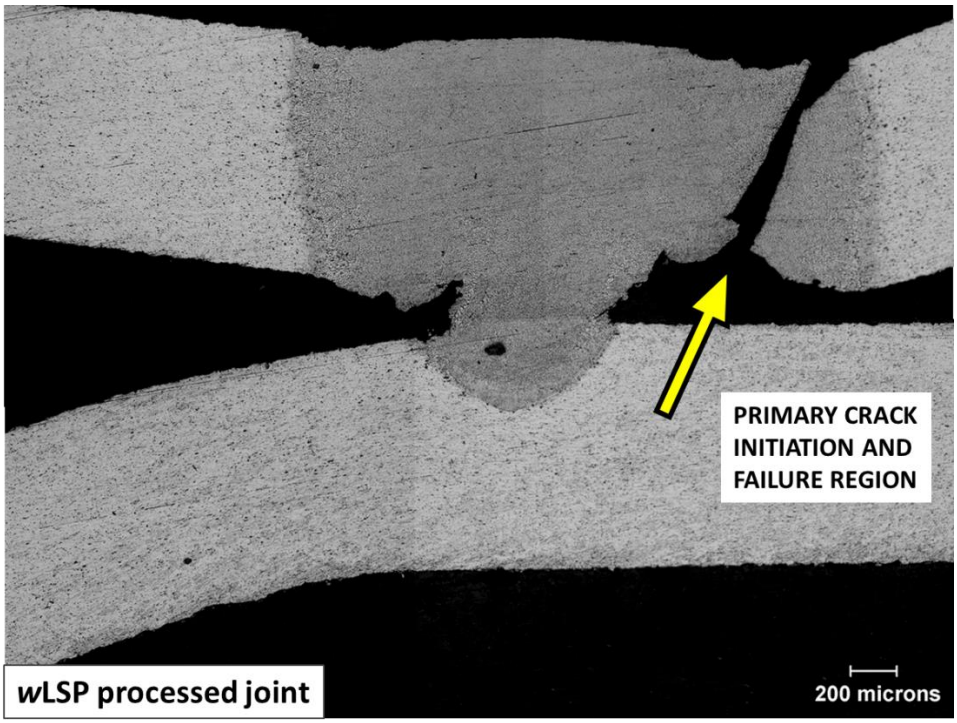

(b)

Figure 3.12. Failure modes for AA6061-T6 lap joints in (a) as-welded condition and (b) wLSP processed condition

3.2.4 Effect of *w*LSP on TZM alloy base material

TZM alloys are a rarely studied material. To the author's best knowledge, there are no investigations reported in literature on the effects of laser shock peening of TZM alloys. To develop a baseline on the impact of rtLSP and *w*LSP processing on TZM alloys, as-received 1mm thick TZM alloy samples were processed with rtLSP and *w*LSP and then tested for uniaxial tensile loading per ASTM E8 standard. The load vs displacement curves for the tested samples are shown in Figure 3.13. The processing of TZM alloy with rtLSP induced compressive residual stresses in the material, thereby increasing its tensile strength; however, some loss of ductility was observed. *w*LSP processed samples improved the tensile strength as well as a significant improvement in ductility Therefore *w*LSP was used to post-process BOP and lap welded joints.

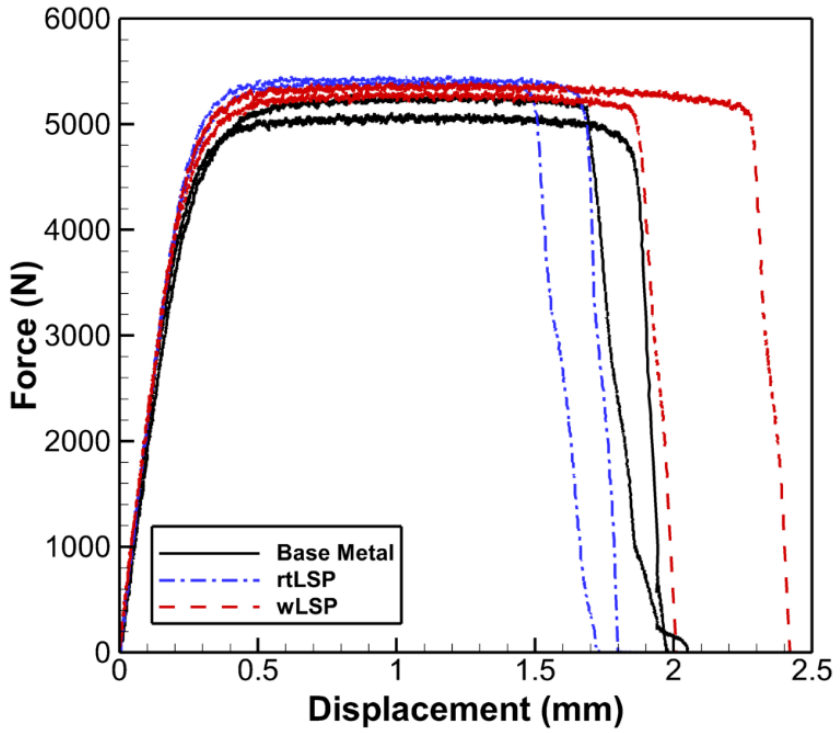

Figure 3.13. Load vs Displacement curves for as received TZM alloy processed with rtLSP and wLSP

3.2.5 Effect of *w*LSP on TZM alloy bead on plate welded joints

TZM alloys lose plasticity and are severely embrittled when welded, resulting in much lower joint tensile strength than the base material, as reported in previous studies [39, 36]. Figure 3.14 shows the change in the mechanical response of the TZM alloy after welding is carried out. Therefore improvement in weld joint strength would be highly desirable.

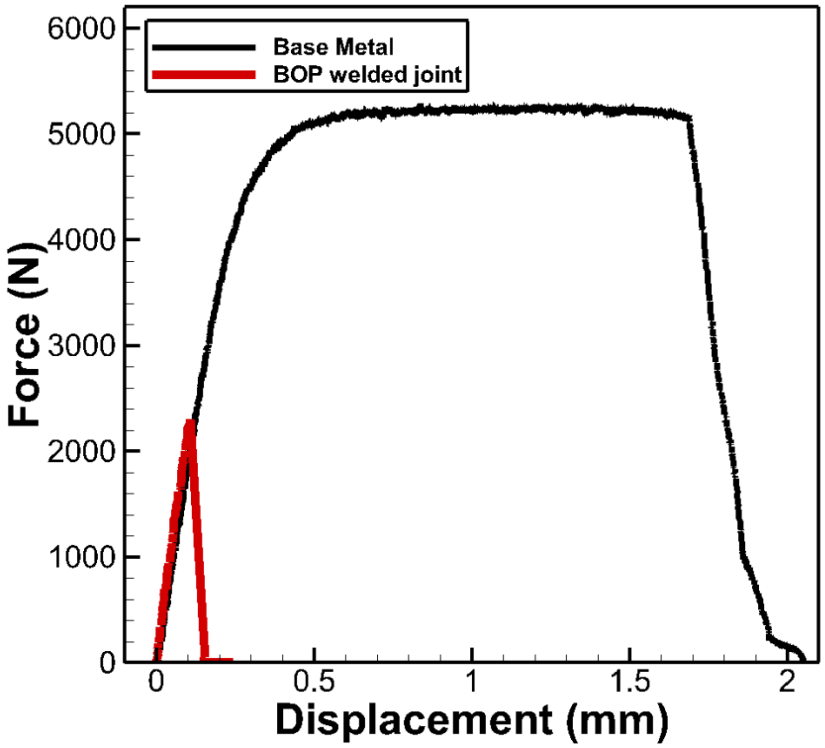

Figure 3.14. TZM alloy mechanical response drastically changes due to welding

Load vs displacement curves for as welded and *w*LSP processed samples are shown in Figure 3.15. From the figure a similar loss in plasticity is observed for welded joints. *w*LSP processing of BOP welds show an improvement in tensile strength of the joint by an average 30% over the as-welded joints. Microhardness measurements for BOP welds are shown in Figure 3.16. Fracture analysis for as-welded and *w*LSP processed samples revealed brittle fracture as shown in Figure 3.17. In the as-welded samples fracture cracks propagate through the coarse columnar grains with lower hardness in between the weld centerline and the heat affected zone. However,

for *w*LSP processed samples, the fracture crack propagates through the center line of the weld nugget, through the equiaxed grains.

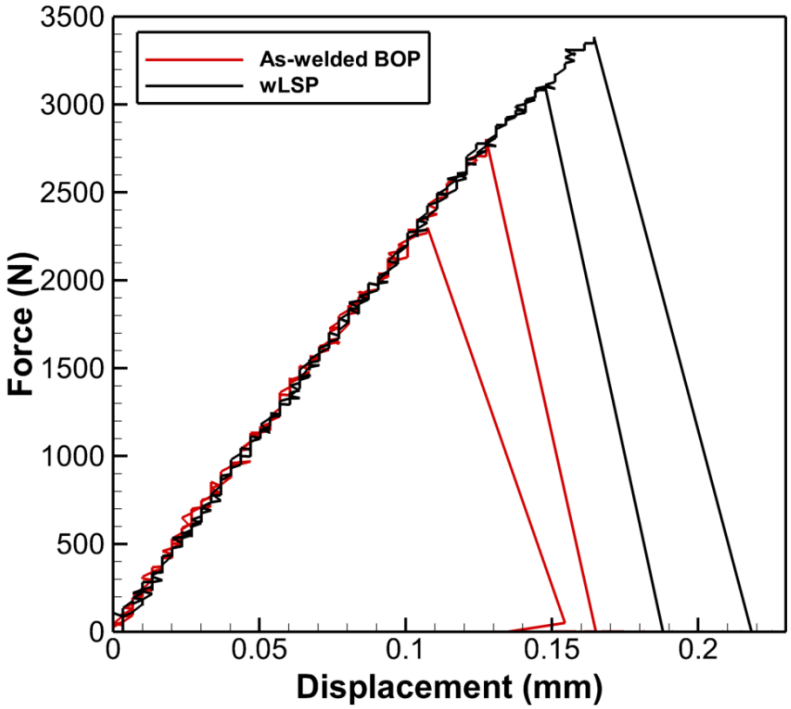

Figure 3.15. Load vs Displacement curves for BOP welded joints processed with wLSP

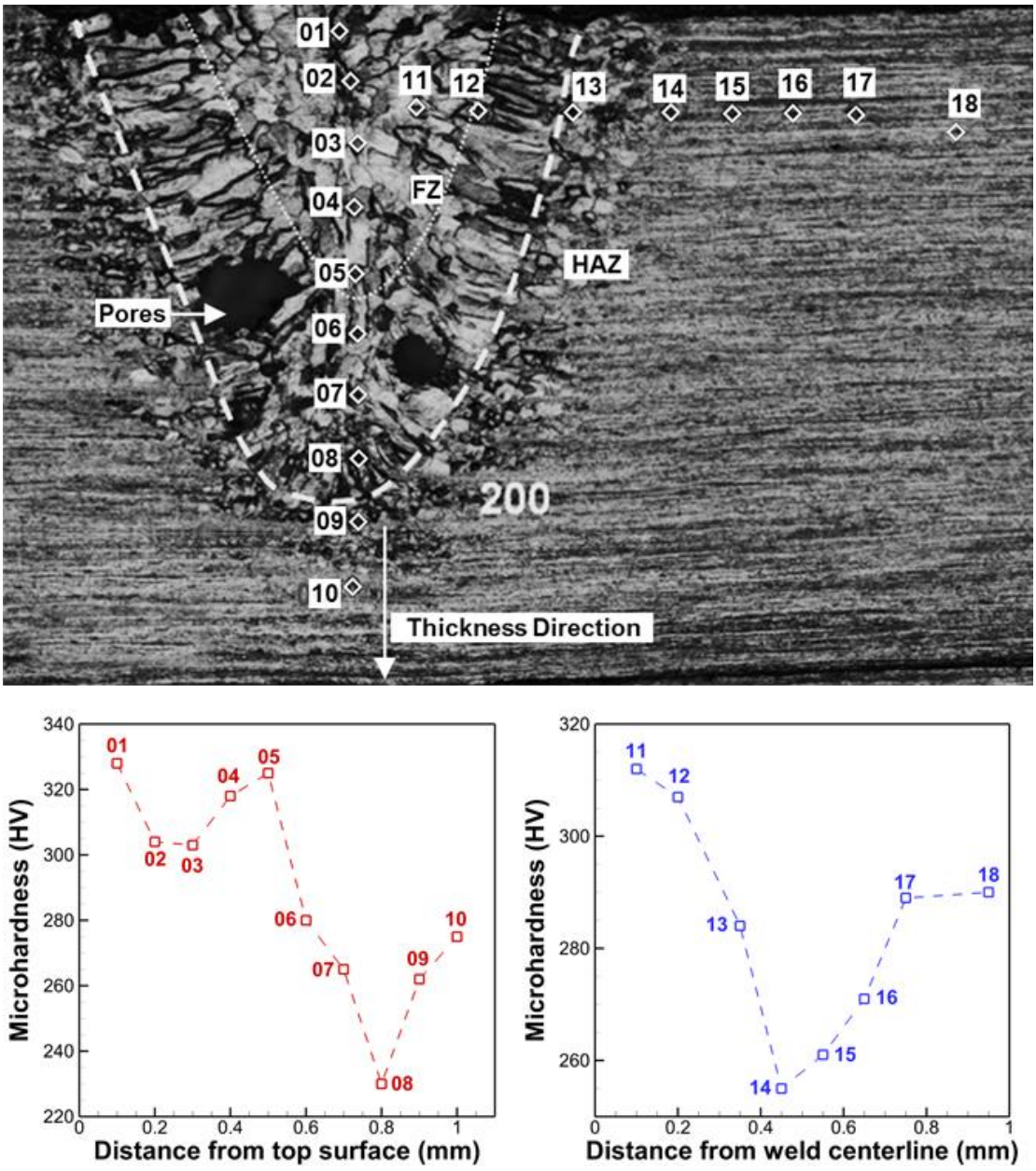

Figure 3.16. Microhardness measurements for BOP welds

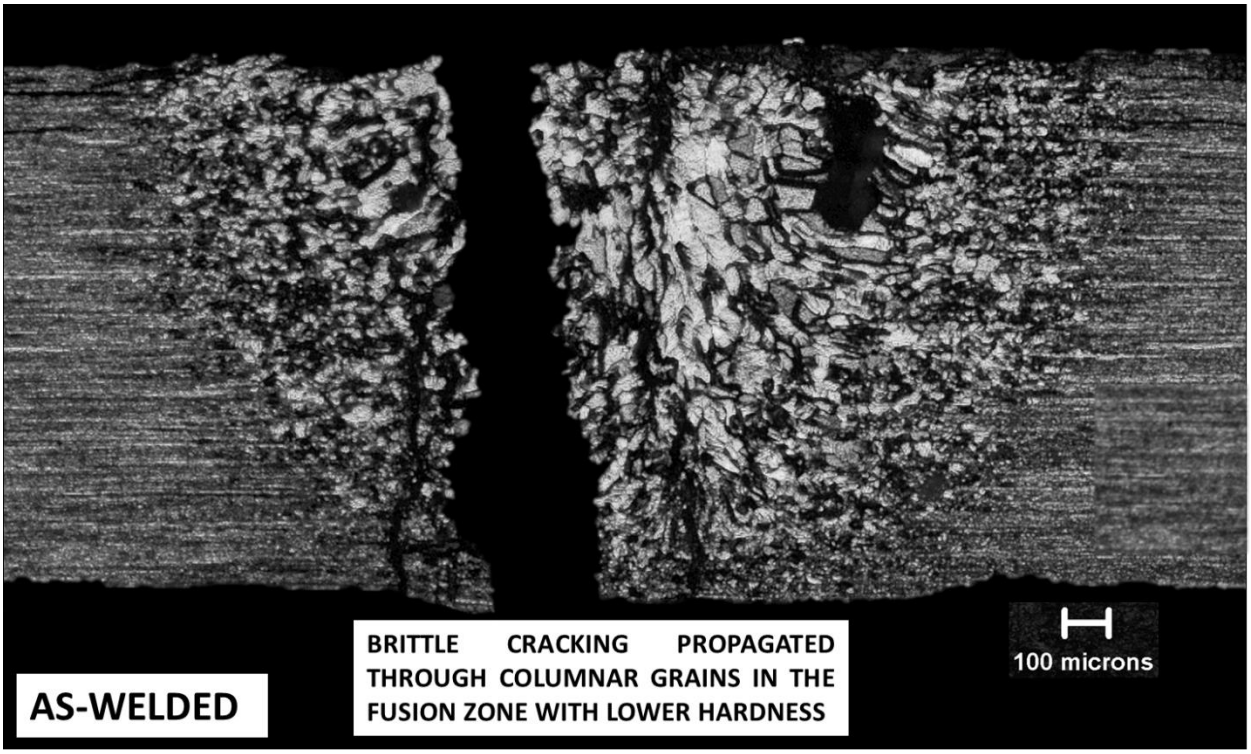

(a)

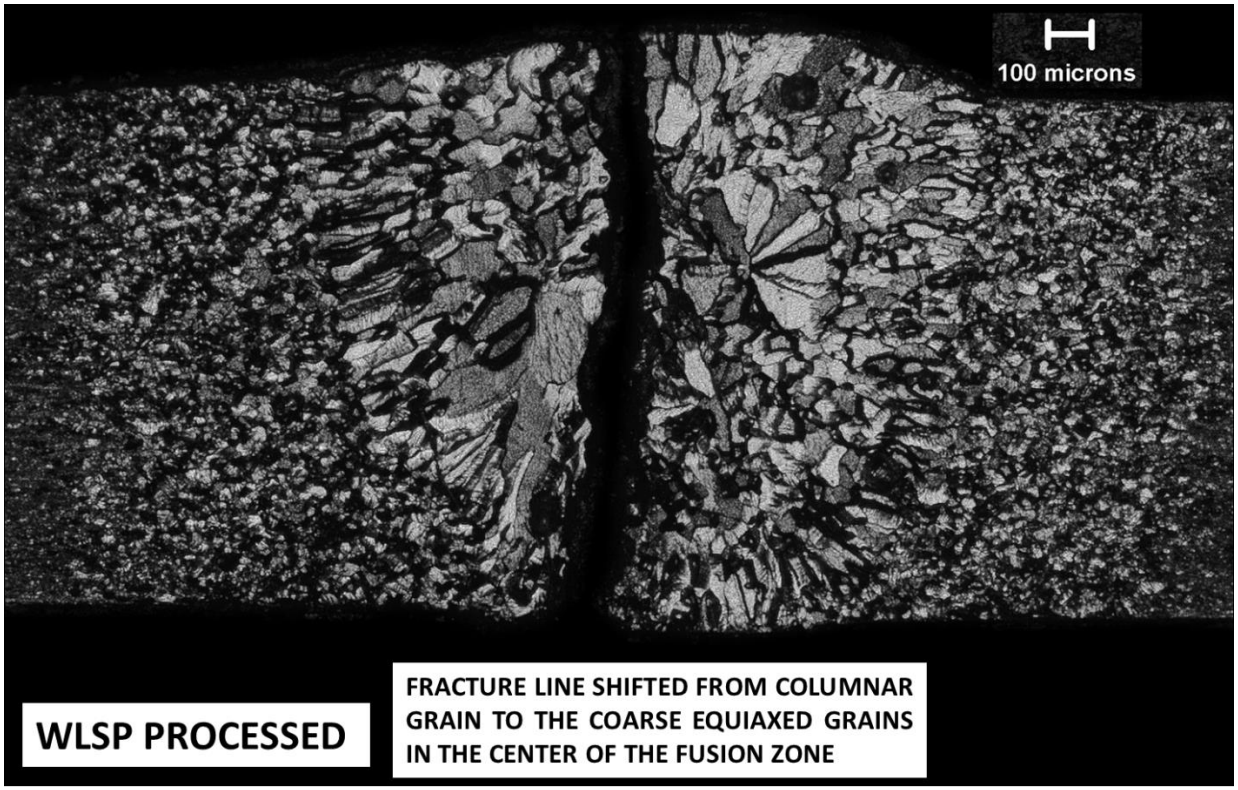

(b)

Figure 3.17. Failure mode for BOP welded joints

3.2.6 Effect of *w*LSP on TZM alloy overlap welded joints

Load vs displacement curves for tensile shear testing of TZM alloy lap welded joints processed with *w*LSP are shown in Figure 3.18. wLSP processed joints sustained higher loads than as-welded samples. As the welded joints display no ductility, it is critical to understand the stress concentrations in the embrittled joints to understand the failure modes in the joints. For this purpose, finite element modeling of the TZM lap welded joint was carried out. The material properties for TZM alloy listed in Section 2.3.1.2 were used for the base material. For the weld region, microhardness tests were carried out, shown in Figure 3.19, and the ultimate tensile strength values were computed. These tensile strength values were used to define material strength in the weld nugget. A schematic for TZM material modeling is shown in Figure 3.20.

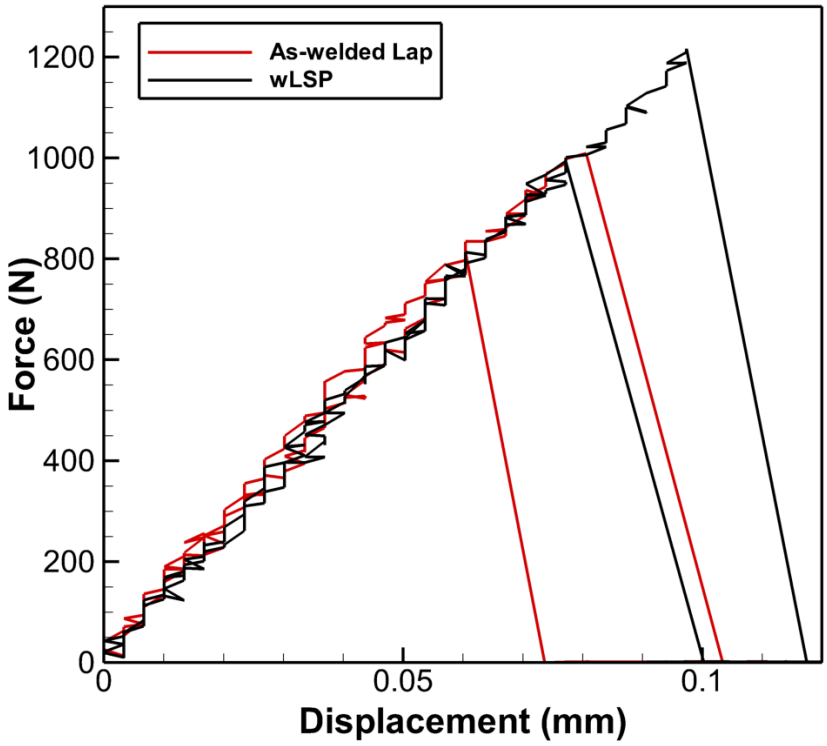

Figure 3.18. Load vs Displacement curves for lap welded joints processed with wLSP

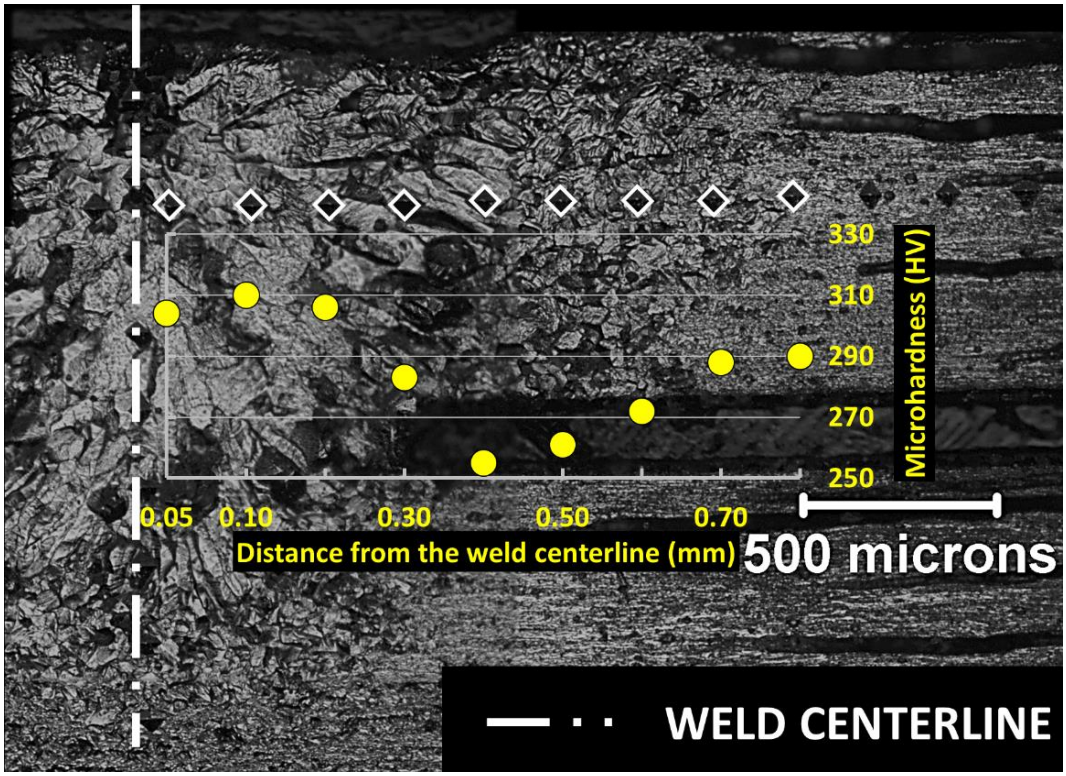

Figure 3.19. Microhardness measurement across weld region for TZM alloy lap weld.

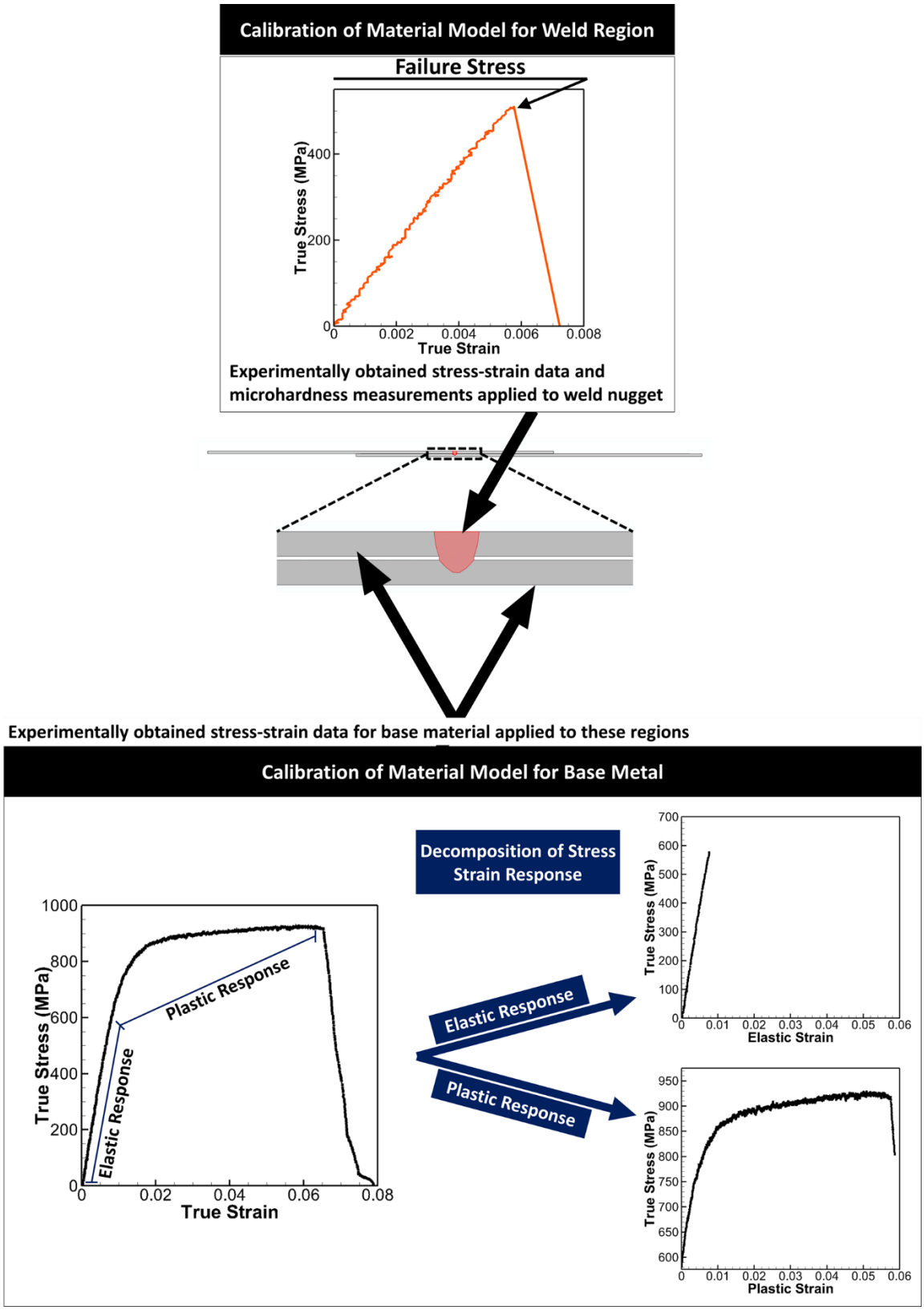

Figure 3.20. Schematic for TZM material modeling using experimental data.

The stress concentration regions predicted by the finite element model are shown in Figure 3.20. From the figure, it can be seen that under a tensile shear loading condition, the primary stress concentration propagates from the interface region towards the top surface of the weld. Secondary fracture occurs at the interface between the top and bottom surface. Due to the lack of ductility, there is no plastic deformation in the sample and the fracture lines indicate pure brittle failure. Failure regions for the as-welded and *w*LSP processed samples were found to be similar and show failures along the stress concentration regions predicted by the finite element model.

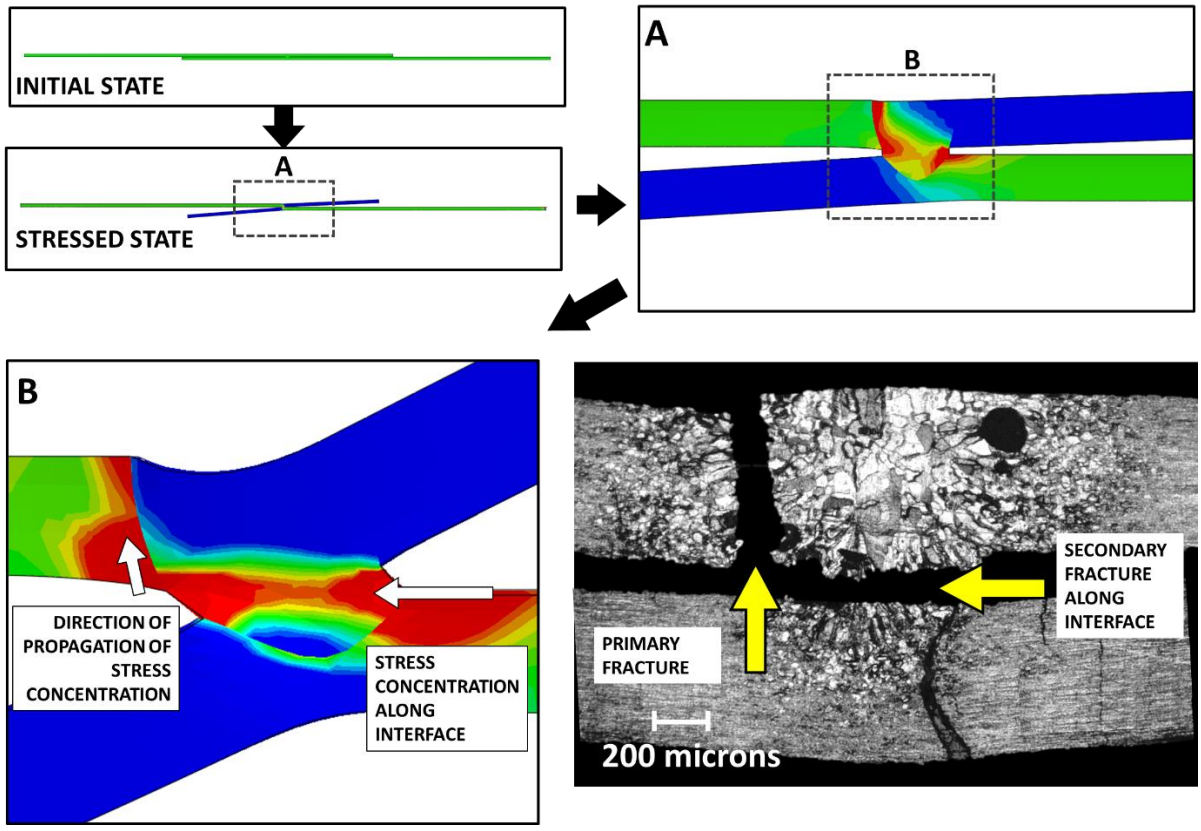

Figure 3.21. Stress concentration regions predicted by finite element modeling of tensile shear loading of TZM alloy lap welds

3.3 Discussions

Laser welded joints of AA6061-T6 and TZM alloy are marred by reduced strength at joint than the base material. Porosity, loss of alloying elements, coarsening of grains, impurity

segregation and embrittlement, are a few reasons that cause the reduction in joint strength. Therefore, post-processing techniques for joint strength enhancement are a critical area of need. *w*LSP is a promising post-processing technique that assists in material strengthening by virtue of dislocation pinning caused by nanoprecipitates interacting with dense dislocations. Dislocations are generated due to the laser shock peening process and the nanoprecipitates are generated due to dynamic precipitation effect caused by elevating material temperature while inducing high strain rate deformations on the material. However the use of *w*LSP in the industry was limited due to the previous studies' use of a heating pad to elevate material temperature. This study aimed to investigate the use of a novel dual laser *w*LSP processing technique that would heat up the material and perform laser shock peening simultaneously. The joint strength of AA6061-T6 BOP and lap welds processed with wLSP are shown in Figures 3.6 and 3.8. Post processing welded joints with *w*LSP resulted in increased joint strength and improved ductility. The joint strength of TZM alloy BOP and lap welds processed with *w*LSP are shown in Figures 3.14 and 3.16. TZM alloys are remarkably difficult to weld and welded joints are marred by a complete loss of plasticity. However, *w*LSP processing of the TZM welded joints resulted in enhanced load capacity of the welded joint and a marginally improved elastic response of the material. There are a few distinct mechanisms that assist in the strengthening of the welded joints while also retaining and improving ductility. *w*LSP induces dislocations in the material subsurface along with dense nanoprecipitates. Under mechanical loading, the dislocation movement is restricted by nanoprecipitates causing the dislocation pinning effect which results in higher strength in the material. The dislocations generated by *w*LSP are however less dense than rtLSP [21], which allow for a retention of ductility.

4. CONCLUSIONS AND RECOMMENDATIONS

4.1 Conclusions

In this research, a novel dual laser warm laser shock peening process has been developed, which is capable of in-situ processing of materials to enhance their mechanical properties. A finite element model has been developed to predict the surface geometry and the compressive residual stresses induced in the material after processing with *w*LSP. Good agreement between the predicted and experimental results for different materials demonstrate a high flexibility of the confined plasma model and the finite element model in predicting mechanical properties for *w*LSP processed materials. The dual laser *w*LSP process was applied on laser welded AA6061-T6 and TZM alloy joints as a post processing weld strengthening technique successfully. Considerable improvement in the joint strength and ductility indicate that this process can be tailored to enhance the joint strength for a range of different welded joints with complex geometries. The key findings and conclusions are as follows:

1. Warm laser shock peening was an effective method of increasing joint strength of laser welded joints, which is known to be a critical area for improvement. The use of a novel dual laser setup for rapid heating and simultaneous *w*LSP is an industrially viable processing technique and can be used to rapidly improve the weld strength of in-situ welded joints.
2. The tensile strength of BOP welded AA6061-T6 alloy processed with *w*LSP was improved by about 20% and the ductility was improved by about 33%.
3. *w*LSP improved the ductility of lap welded AA6061-T6 joints by about 40%. While the failure mode occurred in the HAZ for both the as-welded and *w*LSP processed samples, the dislocation pinning effect and dislocation accumulation capability by *w*LSP contributed to the improved ductility.

4. The tensile strength of BOP welded TZM alloy processed with *w*LSP was improved by about 30% and the weld strength of lap welded TZM alloy processed with *w*LSP was improved by about 22%.
5. Finite element simulations showed deeper compressive residual stresses having a greater magnitude with *w*LSP compared to those of rtLSP. This increased depth of high magnitude compressive stresses assisted in the enhancement of strength of *w*LSP processed laser welded joints.

4.2 Recommendations

A few ideas for future research on the modeling and experimental aspects are summarized as follows:

- The finite element model can be validated for processing of different materials such as low carbon steels, wrought aluminum alloys, titanium alloys, etc
- One of the major advantage of this novel process of rapid heating and simultaneous LSP is the very short processing time. Due to the short time scale, it would be interesting to quantify the dynamic aging effects caused i.e. the size and density of the precipitates generated need to be investigated.
- Thermally engineered LSP is an innovative process in which the processed material is subjected to post shock tempering to tailor the size of the precipitates. The thermal engineered LSP using this dual laser *w*LSP technique would be a very lucrative area of investigation for strengthening of materials due to its flexibility in application.

4.3 Acknowledgement

I thank my colleagues Mr. Luca Pellone, Ms. Jie Ning and Mr. Kyung-Min Hong for their tremendous contribution in determining the welding parameters, carrying out the welding experiments and assisting in the microstructure analysis of the welded samples. I also would like to thank Mr. Sijie Zhang for providing me with the LSP plasma pressure history by using the confined plasma model.

REFERENCES

[1] C. S. Montross, T. Wei, L. Ye, G. Clark and Y. Mai, "Laser shock processing and its effects on microstructure and properties of metal alloys: a review," *International Journal of Fatigue,* vol. 24, no. 10, pp. 1021-1036, 2002.

[2] C. Ye, Y. Liao and G. J. Cheng, "Warm Laser Shock Peening Driven Nanostructures and Their Effects on Fatigue Performance in Aluminum Alloy 6160," *Advanced Engineering Materials,* vol. 12, no. 4, pp. 291-297, 2010.

[3] O. Hatamleh, J. Lyons and R. Forman, "Laser and shot peening effects on fatigue crack growth in friction stir welded 7075-T7351 aluminum alloy joints," *International Journal of Fatigue,* pp. 421-434, 2007.

[4] O. Hatamleh, "Effects of peening on mechanical properties in friction stir welded 2195 aluminum alloy joints," *Materials Science and Engineering: A,* vol. 492, no. 1-2, pp. 168-176, 2008.

[5] Y. Sakino, Y. Sano and Y. Kim, "Application of laser peening without coating on steel welded joints," *International Journal of Structural Integrity,* vol. 2, pp. 332-344, 2011.

[6] L. Zhang, K. Y. Luo, J. Z. Lu, Y. K. Zhang, F. Z. Dai and J. W. Zhong, "Effects of laser shock processing with different shocked paths on mechanical properties of laser welded ANSI 304 stainless steel joint," *Materials Science and Engineering: A,* vol. 528, no. 13-14, pp. 4652-4657, 2011.

[7] X. Chen, J. Wang, Y. Fang, B. Madigan, G. Xu and J. Zhou, "Investigation of microstructures and residual stresses in laser peened Incoloy 800H weldments," *Optics & Laser Technology,* vol. 57, pp. 159-164, 2014.

[8] J. T. Wang, Y. K. Zhang, J. F. Chen, J. Y. Zhou, M. Z. Ge, Y. L. Lu and X. L. Li, "Effects of laser shock peening on stress corrosion behavior of 7075 aluminum alloy laser welded joints," *Materials Science and Engineering: A,* vol. 647, pp. 7-14, 2015.

[9] A. H. Clauer, B. P. Fairand and B. A. Wilcox, "Laser shock hardening of weld zone in aluminum alloys," *Metallurgical Transactions A,* vol. 8, no. 12, pp. 1871-1876, 1977.

[10] S. Malarvizhi and V. Balasubramanian, "Influences of Welding Processes and Post- Weld Ageing Treatment on Mechanical and Metallurgical Properties of AA2219 Aluminum Alloy Joints," *Welding in the World,* vol. 56, no. 9-10, pp. 105-119, 2012.

[11] C. Su, J. Zhou, X. Meng and S. Huang, "Improvement in Fatigue Performance of Aluminium Alloy Welded Joints by Laser Shock Peening in a Dynamic Strain Aging Temperature Regime," *Materials,* vol. 9, no. 10, p. 799, 2016.

[12] W. Braisted and R. Brockman, "Finite Element Simulation of Laser Shock Peening," *International Journal of Fatigue,* vol. 21, pp. 719-724, 1999.

[13] R. Fabbro, J. Fournier, P. Ballard, D. Devaux and J. Virmont, "Physical Study of laser-produced plasma in confined geometry," *Journal of Applied Physics,* vol. 68, no. 2, pp. 775-784, 1990.

[14] L. Zhang and X. Wang, "Hybrid Atomistic-Macroscale Modeling of Long-time Phase Change in Nanosecond Laser-Material Interaction," *Applied Surface Science,* vol. 225, pp. 3097-3103, 2008.

[15] B. Wu and Y. C. Shin, "A Self-Closed Thermal Model for Laser Shock Peening under the Water Confinement Regime Configuration and Comparisons to Experiments," *Journal of Applied Physics,* vol. 97, no. 11, p. 113517, 2005.

[16] K. Ding, "Three-dimensional Dynamic Finite Element Analysis of Multiple Laser Shock Peening Processes," *Surface Engineering,* vol. 19, no. 5, pp. 351-358, 2003.

[17] Y. Hu, Z. Yao and J. Hu, "3-D FEM simulation of laser shock processing," *Surface and Coatings Technology,* vol. 201, no. 3-4, pp. 1426-1435, 2006.

[18] Y. Cao, Y. C. Shin and B. Wu, "A Parametric Study on Overlapping Laser Shock Peening of 4140 Steel via Modeling and Experiments," *Transactions of the ASME, Journal of Manufacturing Science and Engineering,* vol. 132, no. 6, pp. 245-254, 2010.

[19] B. Wu and Y. C. Shin, "From Incident Laser Pulse to Residual Stress: A Complete and Self-Closed Model for Laser Shock Peening," *Transactions of the ASME, Journal of MAnufacturing Science and Engineering,* vol. 129, pp. 117-125, 2007.

[20] Y. Liao, C. Ye and G. J. Cheng, "A review: Warm laser shock peening and related laser processing technique," *Optics & Laser Technology,* vol. 78, pp. 15-24, 2016.

[21] C. Ye, Y. L. Liao, S. Suslov, D. Lin and G. J. Cheng, "Ultrahigh Dense and Gradient Nano-precipitates by Warm Laser Shock Peening for Combination of high Strength and Ductility," *Materials Science & Engineering A,* vol. 609, no. 15, pp. 195-203, 2014.

[22] C. Ye, S. Suslov, B. J. Kim, E. A. Stach and G. J. Cheng, "Fatigue performance improvement in AISI 4140 steel by dynamic strain aging and dynamic precipitation during warm laser shock peening," *Acta Materialia,* vol. 59, pp. 1014-1025, 2011.

[23] J. Z. Zhou, X. K. Meng, S. Huang, J. Sheng, J. Z. Lu, Z. R. Yang and C. Su, "Effects of warm laser peening at elevated temperature on the low-cycle fatigue behavior of Ti6Al4V alloy," *Materials Science and Engineering: A,* vol. 643, pp. 86-95, 2015.

[24] Y. Liao, S. Suslov, C. Ye and G. J. Cheng, "The mechanisms of thermal engineered laser shock peening for enhanced fatigue performance," *Acta Materialia,* vol. 60, no. 13-14, pp. 4997-5009, 2012.

[25] A. Argon, Strengthening mechanisms in crystal plasticity (No. 4), Oxford University Press on Demand, 2008.

[26] K.-M. Hong and Y. C. Shin, "Prospects of laser welding technology in the automotive industry: A review," *Journal of Materials Processing Technology,* vol. 245, pp. 46-69, 2017.

[27] G. Padmanabham and B. Shanmugrajan, "Experimental Investigation of Bead-on-Bead CO2 Laser Welding of Al Alloy 6061," *Trends in Welding Research, Proceedings of the 8th International Conference,* pp. 598-603, 2009.

[28] D. Narsimhachary, R. N. Bathe, G. Padmanabham and A. Basu, "Influence of Temperature Profile during Laser Welding of Aluminum Alloy 6061 T6 on Microstructure and Mechanical Properties," *Materials and Manufacturing Processes,* vol. 29, no. 8, pp. 948-953, 2014.

[29] A. El-Batahgy and M. Kutsuna, "Laser Beam Welding of AA5052, AA5083, and AA6061 Aluminum Alloys," *Advances in Materials Science and Engineering,* p. 9, 2009.

[30] A. Hirose, K. F. Kobayashi and H. Todaka, "CO2 laser beam welding of 6061-T6 aluminum alloy thin plate," *Metallurgical and Materials Transactions A,* vol. 28, no. 12, pp. 2657-2662, 1997.

[31] E. He, J. Liu, J. Lee, K. Wang, D. J. Politis, L. Chen and L. Wang, "Effect of porosities on tensile properties of laser-welded Al-Li alloy: an experimental and modeling study.," *The International Journal of Advanced Manufacturing Technology*, vol. 95, no. 1-4, pp. 659-671, 2018.

[32] G. W. Mugica, D. O. Tovio, J. C. Cuyas and A. C. Gonzales, "Effect of porosity on the tensile properties of low ductility aluminum alloys," *Materials Research*, vol. 7, no. 2, pp. 221-229, 2004.

[33] Q. Chu, R. Bai, H. Jian, Z. Lei, N. Hu and C. Yan, "Microstructure, texture and mechanical properties of 6061 aluminum laser beam welded joints," *Materials Characterization*, vol. 137, pp. 269-276, 2018.

[34] J. K. Kim, H. S. Lim, J. H. Cho and C. H. Kim, "Weldability during the laser lap welding of Al 5052 sheets," *Archives of Materials Science and Engineering*, vol. 31, no. 2, pp. 113-116, 2008.

[35] L. Pellone, G. Inamke, K. M. Hong and Y. C. Shin, "The effects of Interface Gap and Shielding Gas on the Welding Quality during Fiber Laser Lap Welding of AA6061-T6," *Journal of Materials Processing Technology*, vol. 268, pp. 201-212, 2019.

[36] M. Stutz, D. Oliviera, M. Ruttinger, N. Reheis, H. Kestler and N. Enzinger, "Electron Beam Welding of TZM Sheets," *Materials Science Forum*, vol. 879, pp. 1865-1869, 2016.

[37] T. Wang, N. Li, Y. Zhang, S. Jiang, B. Zhang, Y. Wang and J. Feng, "Influence of welding speed on microstructures and mechanicam properties of vacuum electron beam welded TZM alloy joints," *Vacuum*, vol. 149, pp. 29-35, 2018.

[38] T. Wang, Y. Zhang, S. Jiang, X. Li, B. Zhang and J. Feng, "Stress relief and purification mechanisms for grain boundaries of electron beam welded TZM alloy joint with zirconium addition," *Journal of Materials Processing Technology*, vol. 251, pp. 168-174, 2018.

[39] A. Chatterjee, S. Kumar, Tewari R and G. K. Dey, "Welding of Mo-based alloy using electron beam and laser-GTAW hybrid welding techniques.," *Metallurgical and Materials Transactions A*, vol. 47, no. 3, pp. 1-10, 2016.

[40] Y. Zhang, T. Wang, S. Jiang, B. Zhang, Y. Wang and J. & Feng, "Effect of rhenium content on microstructures and mechanical properties of electron beam welded TZM alloy joints," *Journal of Manufacturing Processes,* vol. 32, pp. 337-343, 2018.

[41] K. Elangovan and V. Balasubramanian, "Influences of post-weld heat treatment on tensile properties of friction stir-welded AA6061 aluminum alloy joints," *Materials Characterization,* vol. 59, no. 9, pp. 1168-1177, 2008.

[42] X. Cheng, J. W. Fisher, H. J. Prask, T. Gnaeupel-Herold, B. T. Yen and S. Roy, "Residual stress modification by post-weld treatment and its beneficial effect on fatigue strength of welded structures," *International Journal of Fatigue,* vol. 25, no. 9-11, pp. 1259-1269, 2003.

[43] G. Casalino, M. El Mehtedi, A. Forcellese and M. Simoncini, "Effect of Cold Rolling on the Mechanical Properties and Formability of FSWed Sheets in AA5754-H114," *Metals,* vol. 8, no. 4, p. 223, 2018.

[44] W. Pfeiffer and J. Wensel, "Shot peening of Brittle Materials - Status and Outlook," *Materials Science Forum,* Vols. 638-642, pp. 799-804, 2010.

[45] Y. Sano, K. Masaki, T. Gushi and T. Sano, "Improvement in fatigue performance of friction stir welded A6061-T6 aluminum alloy by laser peening without coating," *Materials & Design (1980 - 2015),* vol. 36, pp. 809-814, 2012.

[46] Y. Tian and Y. C. Shin, "Thermal Modeling for Laser-Assisted Machining of Silicon Nitride Ceramics with Complex Features," *Journal of Manufacturing Science and Engineering,* vol. 128, no. 2, pp. 425-434, 2005.

[47] R. A. Paquin, "Properties of Metals," in *Handbook of optics, vol. IV: Optical properties of materials, nonlinear optics, quantum optics.*, New York, McGraw-Hill, 2010.

[48] Touloukian, Y. S.; Thermophysical and Electronic Properties Information Analysis Center Lafayette IN, Recommended Values of the Thermophysical Properties of Eight Alloys, Major Constituents and Their Oxides, Ft. Belvoir Defense Technical Information Center, 1966.

[49] Smith, D.; International Atomic Energy Agency, ITER blanket, shield and material data base, Vienna: International Atomic Energy Agency, 1991.

[50] B. Wu and Y. C. Shin, "Two Dimensional Hydrodynamic Simulation of High Pressures Induced by High-power Nanosecond Laser-matter Interactions under Water," *Journal of Applied Physics,* vol. 101, p. 103514, 2007.

[51] N. Fang, "Sensitivity analysis of the material flow stress in machining," *ASME 2003 International Mechanical Engineering Congress and Exposition,* pp. 23-32, 2003.

[52] S. Lampman, ASM Handbook. Metallography and Microstructures, Vol. 9, Materials Park, Ohio, USA: ASM, 1990.

[53] "Online Materials Information Resource - MatWeb," MatWeb, 2019. [Online]. Available: http://www.matweb.com/. [Accessed [Online]].

[54] S. A. A. Akbari Mousavi and A. R. Shahab, "Influence of Strain Accumulation on Microstructure of Aluminum 1100 In The Twist Extrusion," *International Journal of Modern Physics B,* vol. 22, no. 18-19, pp. 2858-2865, 2008.

[55] R. Menig, V. Schulze and O. Voehringer, "Optimized warm peening of the quenched and tempered steel AISI 4140," *Materials Science and Engineering: A,* vol. 335, no. 1-2, pp. 198-206, 2002.

[56] Y. Liao, C. Ye, H. Gao, B.-J. Kim, S. Suslov, E. A. Stach and G. J. Cheng, "Dislocation pinning effects induced by nano-precipitates during warm laser shock peening: Dislocation dynamic simulation and experiments," *Journal of Applied Physics,* vol. 110, no. 2, p. 023518, 2011.

[57] J. Ning, K. M. Hong, G. Inamke, Y. Shin and L. Zhang, "Analysis of Microstructure and Mechanical Strength of Lap Joints of TZM Alloy Welded by a Fiber Laser," *Journal of Manufacturing Processes,* p. Manuscript Accepted, 2019.

[58] J. R. Cahoon, W. H. Broughton and A. R. Kutzak, "The determination of yield strength from hardness measurements," *Metallurgical Transactions,* vol. 2, no. 7, pp. 1979-1983, 1971.

[59] H. Kuhn and D. Medlin, "Mechanical Testing and Evaluation," in *ASM Handbook Volume 8,* Materials Park, OH, ASM International, 2000.

[60] C. T. Liu and H. Inouye, "Mechanical properties and interstitial contamination in a molybdenum-base alloy, TZM," Oak Ridge National Laboratory, Tennessee (USA), 1973.

[61] L. Pellone, G. Inamke, K. M. Hong and Y. C. Shin, "The effects of Interface Gap and Shielding Gas on the Welding Quality during Fiber Laser Lap Welding of AA6061-T6," 2018.

[62] H. J. Roven, M. Liu and J. C. Werenskiold, "Dynamic precipitation during severe plastic deformation of an Al–Mg–Si aluminium alloy," *Materials Science and Engineering: A*, Vols. 483-484, pp. 54-58, 2008.

[63] Y. Liao, C. Ye and G. J. Cheng, "[INVITED] A review: Warm laser shock peening and related laser processing technique," *Optics & Laser Technology*, vol. 78, no. A, pp. 15-24, 2016.

[64] J. C. Rozzi, F. E. Pfefferkorn, F. P. Incropera and Y. C. Shin, "Transient, three-dimensional heat transfer model for the laser assisted machining of silicon nitride: I. Comparison of predictions with measured surface temperature histories," *International Journal of Heat and Mass Transfer*, vol. 43, no. 8, pp. 1409-1424, 2000.

[65] G. Tani, L. Orazi, A. Fortunato, A. Ascari and G. Campana, "Warm Laser Shock Peening, New developments and process optimization," *CIRP Annals Manufacturing Technology*, vol. 60, pp. 219-222, 2011.

[66] M. A. Abdulstaar, K. J. Al-Fadhalah and L. Wagner, "Microstructural variation through weld thickness and mechanical properties of peened friction stir welded 6061 aluminum alloy joints," *Materials Characterization*, vol. 126, pp. 64-73, 2017.